Spring tropical cyclones modulate near-surface isotopic compositions of atmospheric water vapour at Kathmandu, Nepal

Niranjan Adhikari[1, 2], Jing Gao[1, 3,*], Aibin Zhao[1], Tianli Xu[1, 4] Manli Chen[1, 3], Xiaowei Niu[1], Tandong Yao[1, 3]

[1] *State Key Laboratory of Tibetan Plateau Earth System, Resources and Environment, Institute of Tibetan Plateau Research, Chinese Academy of Sciences, Beijing 100101, China*

[2] *University of Chinese Academy of Sciences, Beijing 100049, China*

[3] *Lanzhou University, Lanzhou 733000, China*

[4]*Kathmandu Centre for Research and Education,* Chinese Academy of Sciences –*Tribhuvan University, Kirtipur 44613, Kathmandu, Nepal*

* Correspondence to: Jing Gao, E-mail: gaojing@itpcas.ac.cn

Abstract

While westerlies are recognized as a significant moisture transport in Nepal during the pre-monsoon season, precipitation is also attributed to moisture from cyclones originating in the Bay of Bengal (BoB) or the Arabian Sea (AS). Tropical cyclones exhibit negative isotopic values in both precipitation and atmospheric water vapour; however, the factors influencing isotopic fractionation during tropical cyclones remain poorly understood. We present the results of continuous measurements of the isotopic composition of atmospheric water vapour ($\delta^{18}O_v$, δD_v, and d-excess$_v$) at Kathmandu from 7 May to 7 June 2021 during two pre-monsoon cyclones; cyclone Tauktae formed over the Arabian Sea, and cyclone Yaas formed over the Bay of Bengal. Our study reveals that tropical cyclones originating from the BoB and the AS during the pre-

Style Definition: Caption

monsoon season modulate isotopic signals of near-surface atmospheric water vapour in Nepal. Comparing conditions before and after, we observed a significant depletion of $\delta^{18}O_v$ and δD_v during both cyclones, attributed to changes in moisture sources (local vs. marine). Convective activity plays a pivotal role in the variability of $\delta^{18}O_v$ and δD_v during both cyclones, confirmed by the spatial variations of outgoing longwave radiation (OLR) and regional precipitation during both cyclones. We also found a significant negative correlation between $\delta^{18}O_v/\delta D_v$ and rainfall amount along the trajectories during cyclone Tauktae, probably resulting from integrated upstream processes linked to the earlier Rayleigh distillation of water vapour via rainfall, rather than local rainfall. The decrease in $\delta^{18}O_v/\delta D_v$ during cyclone Yaas is associated with the intensified convection and moisture convergence at the measurement site, while the lower cloud top temperatures (CTT) and lower cloud top pressure (CTP) during intense convection contribute to higher d-excess values at the final stage of cyclone Yaas. This characteristic is missing during cyclone Tauktae. Our results shed light on key processes governing the isotopic composition of atmospheric water vapour at Kathmandu with implications for the monsoon moisture transport and paleoclimate reconstructions of tropical cyclone activity.

Keywords: Cyclones; Isotopic composition of atmospheric water vapour; Convection; Moisture convergence; Kathmandu

1 Introduction

Although the Indian summer monsoon accounts for more than 80 % of annual rainfall in Nepal, agricultural activities also rely on precipitation in the pre-monsoon season. Pre-monsoonal rainfall in Nepal is often associated with cyclonic events that provide precipitation to support the timely planting of monsoonal crops. Previous studies have suggested that extreme precipitation in Nepal is mostly fuelled by moisture from the Arabian Sea (AS) and the Bay of Bengal (BoB) (Bohlinger et al., 2017; Boschi and Lucarini, 2019). Higher sea surface temperatures and the westward movement of tropical cyclones formed over the Western Pacific result in cyclones being formed over the BoB and the AS (Mohapatra et al., 2016). The number of cyclones in the AS has increased recently compared to the number of cyclones in the BoB (Pandya et al., 2021). According to the International Best Track Archive for Climate Stewardship (IBTrACS) project (Knapp et al., 2010), in 2019 three cyclones originated in the BoB and five cyclones originated in the AS, due to a rise in sea surface temperature lengthening the cyclone decay period (Li and Chakraborty, 2020). Usually, the impact of cyclones formed over the AS is restricted to the nearest coastal regions. However, in recent years this appears to have changed as cyclones are forming back-to-back over the AS and affecting the entire Indian subcontinent including surrounding regions (Li and Chakraborty, 2020). Cyclone Tauktae affected the livelihoods of people both near the coast and further inland during the pre-monsoon season of 2021 (Pandya et al., 2021). The impacts of cyclone Yaas after cyclone Tauktae were also felt in Nepal, where it triggered flooding and landslides in several parts of the country (https://floodlist.com/asia/nepal-flood-landslide-may-2021/). As both cyclones hit in short succession, this led to severe agricultural damage in several parts of India at a critical time when farmers were preparing to sow their rice paddies ahead of the monsoon season

(https://reliefweb.int/organization/acaps). In Nepal, the damage due to Yaas was mostly limited to the Terai regions which experienced intense and continuous rainfall (https://kathmandupost.com/). Moisture flux associated with cyclones generally extends over a large area and causes moderate to heavy precipitation along the cyclone path and on the nearest land mass (Chan et al., 2022; Rajeev and Mishra, 2022). It is therefore essential to understand the moisture transport processes of these extreme rainfall events on atmospheric water vapour.

With climate change, the amount of water vapour in the atmosphere is also expected to increase, creating scientific interest in the impact of atmospheric water vapour on changing moisture patterns (Hoffmann et al., 2005). The isotopic composition of atmospheric water vapour ($\delta^{18}O_v$, δD_v, and d-excess$_v$) contains comprehensive information about the history of moisture exchange (Noone, 2012; Payne et al., 2007; Risi et al., 2008; Worden et al., 2007). Several studies have shown that isotopic composition is an effective indicator of cyclone activity (Munksgaard et al., 2015; Sun et al., 2022) including cyclone evolution and structure (Lawrence et al., 2002). The atmospheric water vapour and precipitation associated with tropical cyclones tend to have extremely depleted isotopic compositions compared to monsoonal rain (Chen et al., 2021; Jackisch et al., 2022; Munksgaard et al., 2015; Sánchez-Murillo et al., 2019), which may be due to the high condensation efficiency and substantial fractionation associated with cyclones. A few studies found a systematic depletion of heavy isotopes towards the cyclone eye (Lawrence et al., 2002, 1998; Lawrence and Gedzelman, 1996; Sun et al., 2022; Xu et al., 2019). For example, during cyclone Shanshan, Fudeyasu (2008) observed that isotopic depletion in precipitation and water vapour increased radially inward in the cyclone's outer region, likely due to a rainout effect. A study conducted in north-eastern Australia during cyclone Ita in April 2014 underlined the role of synoptic-scale meteorological settings in determining the isotopic

variability of atmospheric water vapour (Munksgaard et al., 2015). In Fuzhou, China, Xu et al., (2019) reported a significant depletion in typhoon rain $\delta^{18}O$ related to the combined effect of large-scale convection, high condensation efficiency, and recycling of isotopically depleted vapour in the rain shield area. Sánchez-Murillo et al., (2019) highlighted the role of convective and stratiform activity as well as precipitation type and amount. The impact of high stratiform fractions and deep convection on isotopic depletion in precipitation during typhoon Lekima was confirmed by Han et al., (2021).

Although several studies have examined the isotopic variation of event-based precipitation in Nepal (Acharya et al., 2020; Adhikari et al., 2020; Chhetri et al., 2014), there remains a knowledge gap regarding the isotopic response of atmospheric water vapour during cyclone events. We present for the first time the evolution of the isotopic composition of atmospheric water vapour ($\delta^{18}O_v$, δD_v, and d-excess) in Kathmandu during~~including~~ two pre-monsoon cyclone events. Isotopic data were collected in 2021, from one week before to one week after the cyclones. A~~lthough neither cyclone passed directly over Kathmandu, their remnant vapour produced several days of rainfall~~ substantial influence of these cyclone events on the sampling sites for several days was apparent in the isotopic composition of atmospheric water vapour, showcasing a marked depletion in comparison to normal days. This allowed us to scrutinize fluctuations in isotopic composition with a high temporal resolution and to investigate the atmospheric processes associated with cyclone events that lead to significant depletion in isotopic composition at diurnal scales. ~~that allowed us to observe changes in the isotopic composition at high temporal resolution and evaluate the cause of such changes at diurnal scales.~~

2 Data and methods

2.1 Site description

The Kathmandu station lies on the southern slope of the Himalayas (27°42′ N, 85°20′ E) at an altitude of approximately 1400 m above sea level. Based on an 18-year-long record from the Department of Hydrology and Meteorology, Government of Nepal (2001 to 2018), this region has an average annual temperature of 19° C and average annual precipitation amount of about 1500 mm, with ~78% of the annual rainfall occurring in the monsoon season from June to September (Adhikari et al., 2020). About 16 % of annual rainfall in Kathmandu occurs in the pre-monsoon season (March to May) with air temperature ~~ranges~~ ranging from 13 to 28° C and is averaged relative humidity (RH) of 67 %. Advection of the southern branch of westerlies and evaporation from nearby water bodies are the main contributors to pre-monsoonal precipitation (Yu et al., 2015; Chhetri et al., 2014). These arid westerlies, resulted in diminished temperature and relative humidity (RH) within the region while a substantial presence of moisture was observed over extensive areas encompassing the BoB, the AS, India, and surrounding regions including our sampling site during our study period. Figure S3~~1~~ shows the elevated specific humidity levels ~~averaged between 1000 hPa and~~at 850 ~~hPa throughout the duration of~~from May to June 7, 2021~~our study period~~.

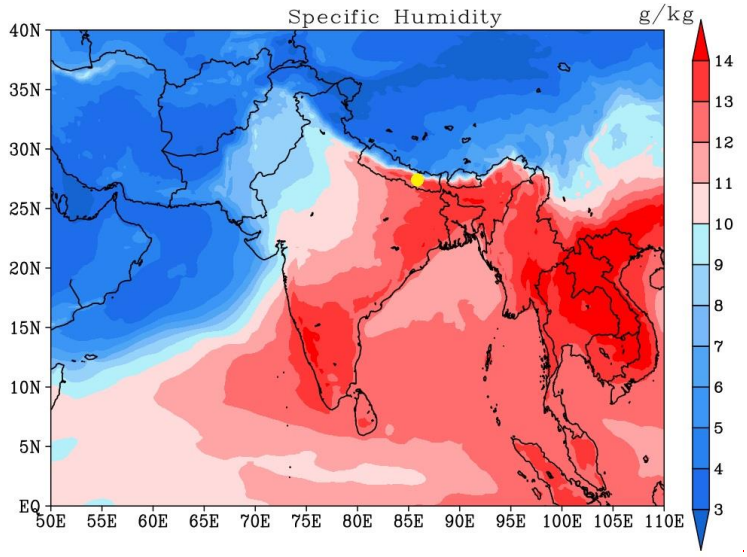

~~**Figure 1 Spatial distribution of specific humidity averaged over 1000 hPa to 850 hPa (in g/Kg) during the period of study. The yellow dot shows the location of Kathmandu.**~~

2.2 The evolution of cyclones Tauktae and Yaas and weather conditions at Kathmandu

Cyclone Tauktae developed as a tropical disturbance on 13 May 2021 over the AS, evolved into a deep depression by 14 May, moved north, and gradually intensified before turning into a cyclonic storm with wind speeds reaching 75 km/h on that same day (Pandya et al., 2021). After making landfall in the Gir-Somnath district of Gujarat, Tauktae continued to strengthen and was classified as an extremely severe cyclonic storm on 17 May reaching maximum wind speeds of 220 km/h (Verma and Gupta, 2021; Pandya et al., 2021). Tauktae weakened into a low depression on 18 May 2021 at 17:00 h Indian Local Time (ILT) and finally dissipated one day later. Due to its large convective area, it brought heavy rainfall to different regions of India and Nepal.

The signal of cyclone Tauktae was first detected at the Kathmandu site on 19 May at approximately 03:00 local time (LT), followed by light drizzle. The recorded air temperature was about 22°C, and the relative humidity (RH) was approximately 72%. Within 16 hours, the RH increased from 72% to 91%, while the temperature dropped from 22°C to around 19°C. The maximum RH and minimum temperature were observed on 21 May around 04:00 h LT, reaching 92% and 17°C, respectively.

Cyclone Yaas started out as a depression over the BoB on 22 May 2021 at 08:30 h ILT and gradually intensified into a deep depression before turning into a cyclonic storm on 24 May at 00:00 h ILT as it moved northeast (Paul and Chowdhury, 2021). The corresponding wind speed and central pressure were recorded as 65 km/h and 990 hPa, respectively. On 24 May around 18:00 h ILT, it intensified into a severe cyclonic storm with wind speeds ranging from 89 to 117 km/h before becoming a very severe cyclonic storm on 25 May at 12:00 h ILT with wind speeds from 119 km/h to 165 km/h. It made landfall north of Odisha on 26 May with maximum sustained wind speeds of 130 km/h to 140 km/h and progressively weakened into a depression on 27 May before dissipating over northern India on 28 May.

The Kathmandu weather station recorded a total of 59.6 mm of precipitation during cyclone Yaas. Intermittent small patches of rainfall commenced on 25 May at 11:00h LT. The main cyclone event occurred from 26 May at 01:00h LT to 29 May at 01:00h LT. Throughout this period, the ground-level RH fluctuated between 84% and 93%, while surface temperature varied between 18°C and 22°C. Notably, all RH values exceeded 80% from 25 May around 22:00 h LT to 29 May at 10:00 h LT.

Wind speeds, pressure, and cyclone eye location information (3-hour resolution) were retrieved from the best track data of tropical cyclonic disturbance over the north Indian Ocean (available at https://rsmcnewdelhi.imd.gov.in/) monitored by India Meteorological Department (IMD)~~taken from datasets of the International Best Track Archive for Climate Stewardship (IBTrACS) project (Knapp et al., 2010), https://www.ncei.noaa.gov/products/).~~ . The latter was used to calculate the spatial distance between the cyclone's eye and our measurement location. Figure ~~2~~1 illustrates the intensity and cumulative rainfall along the paths of the cyclones. A characteristic of both cyclones is the occurrence of rainout along their trajectories, persisting as they move inland.

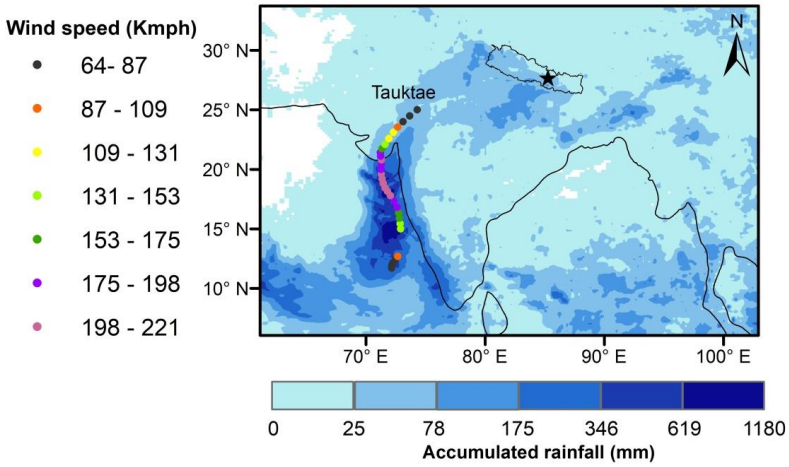

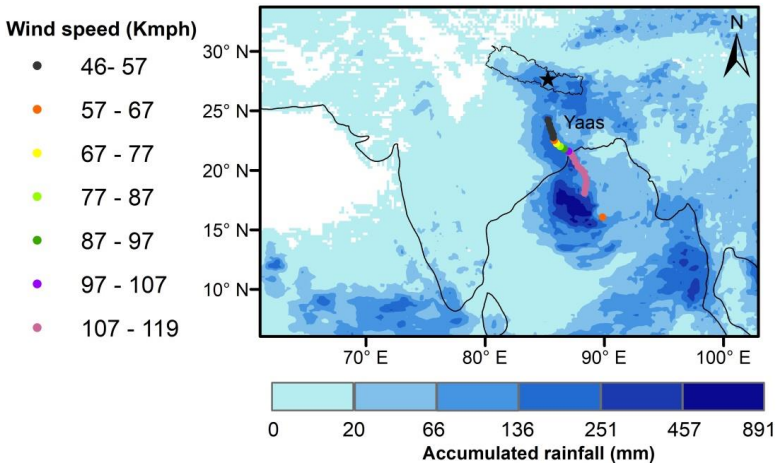

171

172 **Figure 12 The intensity and track of cyclone Tauktae (Upper panel) and Yaas (Bottom**
173 **panel) along with accumulated rainfall during Tauktae (from 14 to 20 May 2021) and Yaas**
174 **(24 to 28 May 2021)their occurrence. The intensity and track of cyclones were retrieved**
175 **from the best track data of tropical cyclonic disturbance over the north Indian Ocean**
176 **monitored by IMD and rainfall data was retrieved from the Integrated Multi-satellite**

Retrievals provided by the Global Precipitation Measurement program (GPM, IMERG dataset).

2.3 Isotope measurements

Near-surface $\delta^{18}O_v$ and δD_v were measured continuously using a Picarro L2130-i analyser based on wavelength-scanned cavity ring-down spectroscopy (WS-CRDS) (Brand et al., 2009), located at the Kathmandu Centre for Research and Education (KCRE), Nepal. The sampling inlet consisting of a heated copper tube mounted 7 m above the ground protected with a plastic hood and a 10 L min^{-1} pump transported the sample from the inlet to the analyser. The automated standard delivery module (SDM) was used for calibration, with each calibration made using two reference standards calibrated against Vienna Standard Mean Ocean Water (VSMOW), covering the isotopic ranges of ambient water vapour at Kathmandu. Each reference standard was measured continuously for a total of 75 min each day at three different humidity levels (25 minutes per level). The dry air passed through Drierite™ desiccant (Merck, Germany) and was delivered to the Picarro analyser for standard measurements. The isotopic composition of atmospheric water vapour is reported as parts per thousand (‰) relative to VSMOW using

$$\delta^{*} = (R_A / R_S - 1) \times 1000\ [‰], \quad (1)$$

where δ^{*} represents either δD_v or $\delta^{18}O_v$, and R_A and R_S denote the ratios of heavy to light isotopes ($^{18}O/^{16}O$ or D/H) in the sample and standard, respectively (Kendall & Caldwell, 1998; Yoshimura, 2015). As suggested by Dansgaard, (1964), deuterium excess ($d\text{-}excess_v = \delta D_v - 8 \times \delta^{18}O_v$) is used as a tracer for moisture source conditions (Liu et al., 2008; Tian et al., 2001). The detailed calibration procedures are outlined in the supplementary material, with the humidity-

isotopes response function presented in Figure S2 and all calibration data shown in Figure S3. We examined the hourly isotopic composition of atmospheric water vapour between 7 May and 7 June 2021, covering the Tauktae and Yaas cyclones including one week on either side.

2.4 Meteorological data

An automated weather station (AWS, Davis Vantage Pro2) continuously measured air temperature, relative humidity, dew point temperature, wind speed and direction, rainfall amount, surface pressure, etc. at one-minute intervals from 7 May to 7 June 2021.

We used the Integrated Multi-satellite Retrievals provided by the Global Precipitation Measurement program (GPM, IMERG dataset)~~We used Integrated Multi-satellite Retrievals for GPM (IMERG) from the Global Precipitation Measurement (GPM) program~~ with a spatial resolution of 0.1° for latitude and longitude (Huffman et al., 2017) to analyse the regional rainfall intensity before, during, and after the cyclone events. These high-resolution data allow for the identification of convective rainfall areas and the passage of tropical cyclones (Jackisch et al., 2022). They have been used previously to depict cyclone tracks and associated rainfall intensities (Gaona et al., 2018; Jackisch et al., 2022; Villarini et al., 2011).

We further acquired data on outgoing longwave radiation (OLR), zonal and meridional winds, specific humidity, vertical velocity, pressure, vertical distribution of relative humidity and temperature from ERA5 datasets (Herbash et al., 2020). The data has a spatial resolution of 0.25° based on longitude-latitude grids ~~We further obtained outgoing longwave radiation (OLR), zonal and meridional wind, specific humidity, vertical velocity, pressure, and distribution of relative humidity and temperature data from ERA5 datasets (Herbash et al., 2020) with a spatial resolution of 0.25° from longitude-latitude grids~~ (https://cds.climate.copernicus.eu/). OLR data has already been used as an index of tropical convection (Liebmann and Smith, 1996).

Additionally, we used cloud-top pressure (CTP) and cloud-top temperature (CTT) data from MERRA-2 Reanalysis datasets retrieved from https://giovanni.gsfc.nasa.gov/, with a spatial resolution for~~of~~ 0.5°×0.625°, as indicators of convective intensity.

2.5 Moisture backward trajectory analysis

To assess the influence of moisture transport history on the isotopic composition of atmospheric water vapour before, during, and after the cyclone events, we analysed five-day moisture backward trajectories that terminated at the sampling site using the Hybrid Single-Particle Lagrangian Integrated Trajectory (HYSPLIT) model (Draxler and Hess, 1997). The Global Data Assimilation System (GDAS) with a spatial resolution of 1° (Kleist et al., 2009) was used to provide the meteorological forcing for the HYSPLIT model. Variations in specific humidity along the moisture trajectories were also calculated. Considering the variation in boundary layer height at Kathmandu during the study period, ranging from approximately 100 m to 1170 m, and with the majority of the data falling below 600 m, we set the initial starting height for the moisture backward trajectories to 500 m above ground.

3 Results and discussion

~~3~~3.1 Isotope dynamics and their relation with local weather before, during, and after cyclone events

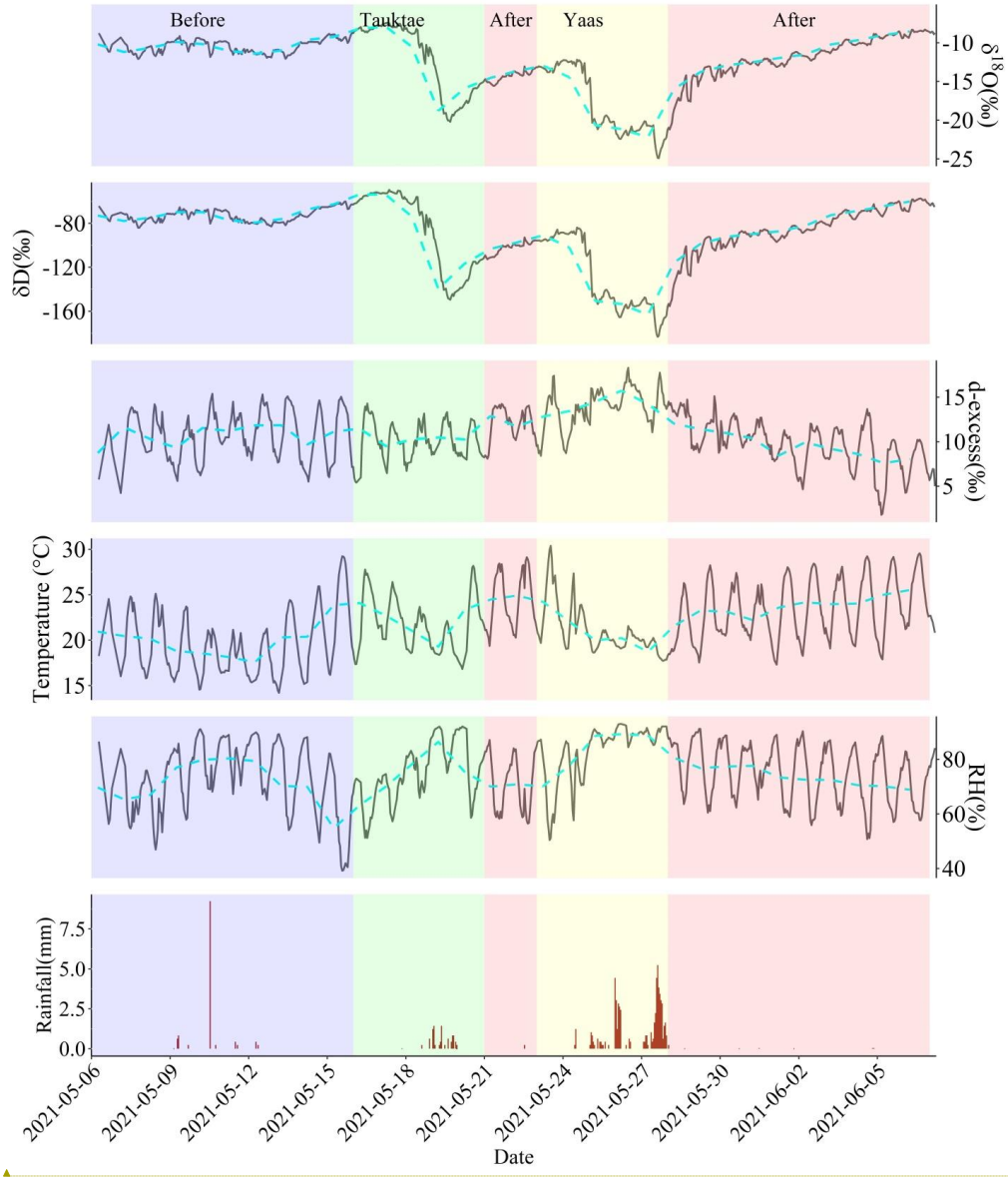

Formatted: Heading 2

Formatted: Font: 12 pt, Not Bold

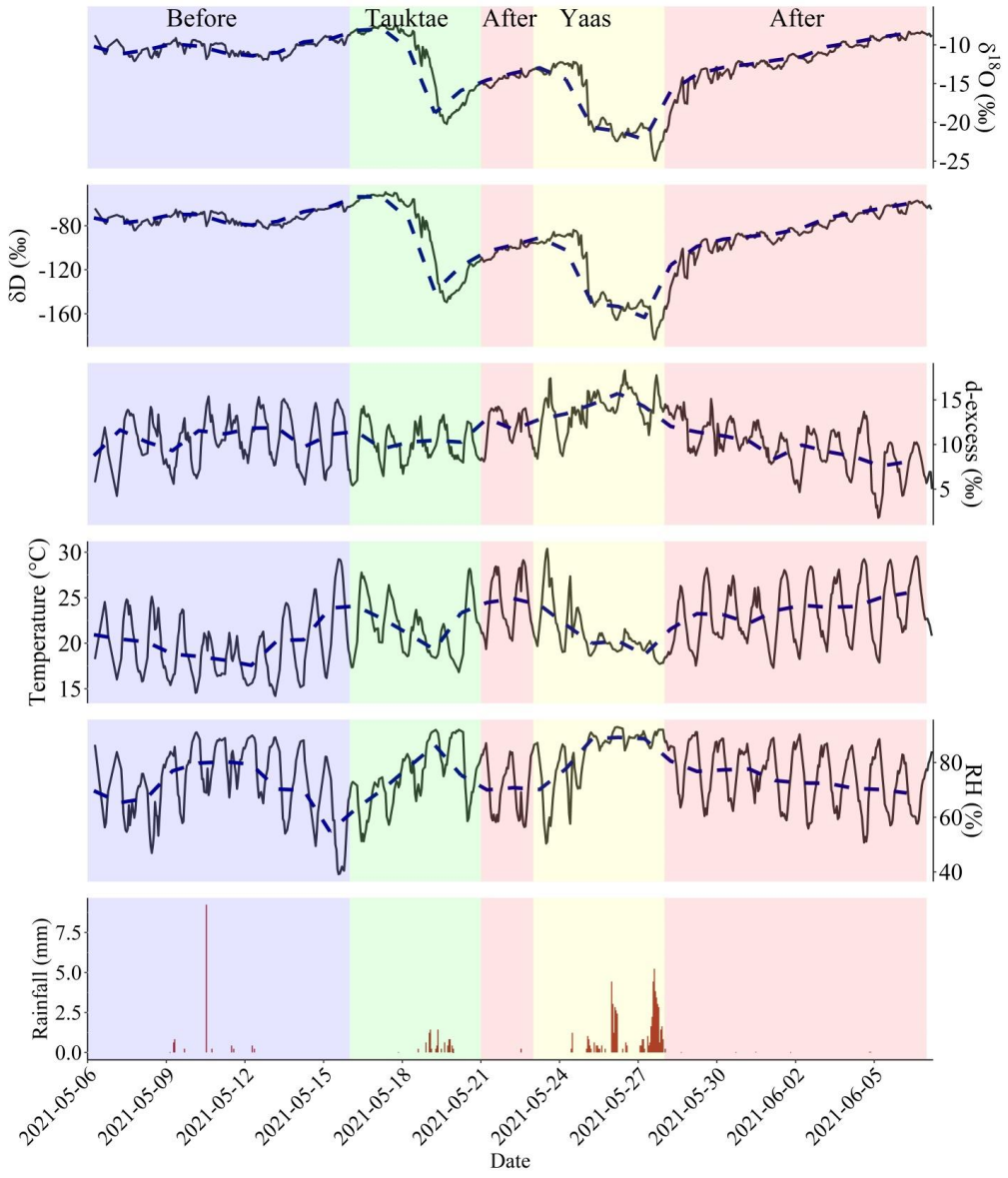

241

242 **Figure 23 Water vapour isotopic evolution (hourly averages) before, during, and after the**

243 **Tauktae and Yaas cyclone events as indicated by the colour shading along with associated**

Formatted: Font: 12 pt, Not Bold

surface air temperature, relative humidity (RH), and rainfall amount. The blue~~cyan~~ dashed line represents daily average~~variations~~.

Significant variability was observed in isotopic composition before, during, and after the cyclones at Kathmandu station (Figure 2~~Fig. 3~~2 and Table 1~~Table 1~~). $\delta^{18}O_v$ and δD_v showed a sudden depletion in isotopic composition the final stages of both cyclones, coinciding with RH reaching maximum values. The depletion was more pronounced during cyclone Yaas compared to cyclone Tauktae.

Before the cyclone Tauktae, $\delta^{18}O_v$ (δD_v) varied from -7.40 ‰ (-49.53 ‰) to -12.10 ‰ (-84.15 ‰) with an average of -10.04 ‰ (-69.51 ‰) and d-excess$_v$ ranged from 4.24 ‰ to 15.38 ‰ with an average of 10.84 ‰. The isotopic composition clearly shows a downward trend as the remnant of cyclones passed over Kathmandu. $\delta^{18}O_v$ decreased by over 12 ‰ from 14 May to 20 May (Tauktae) and again between 24 May and 29 May (Yaas), reaching minima for $\delta^{18}O_v$ (δD_v) of -20.21 ‰ (-149.49 ‰) and -24.92 ‰ (-183.34 ‰), respectively. During Tauktae, $\delta^{18}O_v$ (δD_v) varied from -8.20‰ (-56.06‰) to -20.21‰ (-149.49‰) with an average of -14.73‰ (-106.76‰) and during Yaas the range was~~$\delta^{18}O_v$ (δD_v) ranges~~ from -12.17‰ (-83.85‰) to -24.92‰ (-183.34‰) with an average of -17.87‰ (-129.18‰). Similarly, d-excess$_v$ during Tauktae varied from 7.97 ‰ to 14.24 ‰ with an average of 11.06 ‰ while during Yaas it varied from 8.71 ‰ to 18.29 ‰ with an average of 13.77 ‰. After both cyclones had dissipated, $\delta^{18}O_v$ (and δD_v) started to recover pre-cyclone values of -8.29 ‰ to -14.94 ‰ (-57.40 ‰ to -109.31 ‰), with an average of -11.09 ‰ (-79.38 ‰), and a d-excess ranged between 1.80 ‰ and 15.11 ‰ with an average of 9.37 ‰.

The remnants of cyclone Tauktae caused light rain at Kathmandu, with a significant depletion in $\delta^{18}O_v$ (δD_v) by ~8 ‰ (~66 ‰) on 20 May compared to the previous day. From the formation of a depression over the AS on 14 May 2021 until the dissipation inland on 19 May ~~(Fig. S3)~~, no significant variation in the isotopic composition in atmospheric water vapour at Kathmandu was observed (Fig. 2~~3~~). After the dissipation, when the residual Tauktae vapour passed the Kathmandu site producing light rains, $\delta^{18}O_v$ and δD_v began to decrease independently of the rainfall amount, starting on 19 May around 11:00 h Local Time (LT), from -8.34 ‰ for $\delta^{18}O_v$ and -56.06 ‰ for δD_v and decreasing in one hour to -10.12 ‰ and -68.41 ‰ respectively. This decrease continued for 24 hours reaching a minimum of -20.21 ‰ and -149.49 ‰ for $\delta^{18}O_v$ and δD_v respectively on 20 May at 12:00 h LT. However, d-excess$_v$ did not show notable variations during the passage of cyclone Tauktae. $\delta^{18}O_v$ and δD_v remained depleted from 20 to 22 May.

On 24 May, cyclone Yaas formed over the BoB and followed a trajectory through north-eastern India ~~(Fig. S4)~~. The effect of cyclone Yaas on $\delta^{18}O_v$ and δD_v at Kathmandu was observed on 25 May with $\delta^{18}O_v$ (δD_v) dropping rapidly from -12.62 ‰ (-88.71 ‰) on 25 May at 20:00 h LT to -15.07 ‰ (-106.22 ‰) just one hour later. At the same time, d-excess$_v$ increased from 12.30 ‰ to 14.34 ‰. The depletion continued until 28 May with a minimum of $\delta^{18}O_v$ (δD_v) by -24.92 ‰ (-182.35 ‰) at 16:00 h LT. Yaas had already weakened into a low-pressure area over Bihar in south-eastern Uttar Pradesh, India. $\delta^{18}O_v$ and δD_v started to increase by about 10 ‰ on 29 May at 16:00 h LT after Yaas had dissipated. From 25 to 29 May, d-excess$_v$ gradually increased as opposed to $\delta^{18}O_v$ and δD_v, resulting in a negative correlation with $\delta^{18}O_v$ and δD_v of -0.60 and -0.55 respectively.

The passage of cyclones that had formed over the AS (Tauktae) and BoB (Yaas) caused significant depletion in the isotopic composition and led to cumulative rainfall of 9.2 mm (Tauktae) between 14 May and 20 May 2021 and 59.6 mm (Yaas) between 25 May and 28 May 2021 at our site. This depletion is due to cyclone-associated intense rainfall and agrees with previous studies (Krishnamurthy and Shukla, 2007; Rahul et al., 2016). Note the above $\delta^{18}O_v$ minimum (-24.92 ‰) observed during cyclone Yaas is similar to the minima observed in Bangalore, India ($\delta^{18}O_v$ =-22.5 ‰) (Rahul et al., 2016) and Roorkee, India ($\delta^{18}O_v$ =-25.35 ‰) (Saranya et al., 2018) when cyclones evolved over the BoB passed near their sampling sites. These results indicate a similar oceanic source of moisture during cyclones. We discuss the influence of moisture sources in Sect. 3.2~~4.1~~.

The relation between $\delta^{18}O_v$ and δD_v varies for the periods before, during, and after the cyclones, showing different slopes and intercepts with the Local Meteoric Vapour Line (LMVL) (Figure 3~~Fig. 4~~3). Before the first event, both the slope (5.85) and intercept (-12.12) are significantly lower indicating the strong influence of non-equilibrium processes such as evaporation. During both cyclones the slopes and intercepts resemble those of the global meteoric water line (GMWL: $\delta D=8\times\delta^{18}O+10$) (Figure 3~~Fig. 4~~3). After the cyclones the slope and intercept decreased to 7.37 and 2.34 respectively, implying a change of moisture sources and evaporation.

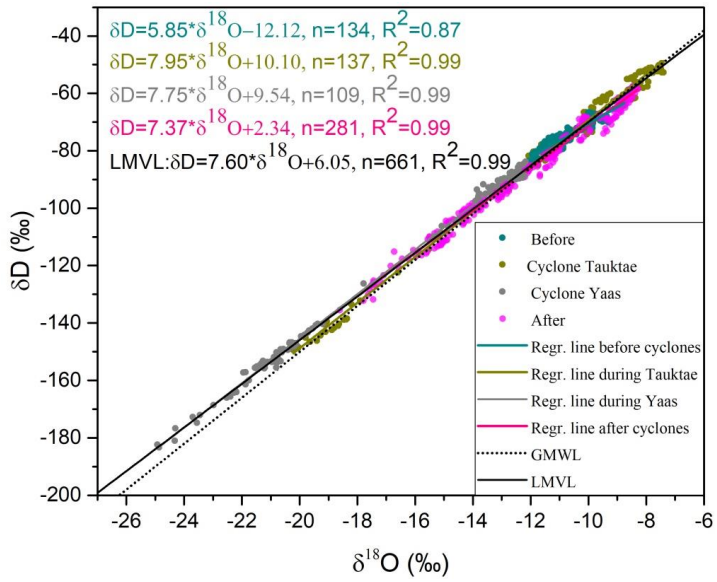

Figure 34 Relationships between $\delta^{18}O_v$ and δD_v before, during, and after the cyclone events. The regression lines for each period are presented along with GMWL for comparison.

Table 1 Descriptive statistics of $\delta^{18}O_v$, δD_v, and d-excess$_v$ measured before, during, and after the cyclone events.

Period	$\delta^{18}O_v$ [‰]			δD_v [‰]			d-excess$_v$ [‰]		
	min	max	avg	min	max	avg	min	max	avg
Before	-12.10	-7.40	-10.04	-84.15	-49.53	-69.51	4.24	15.38	10.84
Cyclone Tauktae	-20.21	-8.20	-14.73	-149.49	-56.06	-106.76	7.97	14.24	11.06
Cyclone Yaas	-24.92	-12.17	-17.87	-183.34	-83.85	-129.18	8.71	18.29	13.77
After	-14.94	-8.29	-11.09	-109.31	-57.40	-79.38	1.80	15.11	9.37

To assess the meteorological influence on the isotopic composition at Kathmandu, we examined the linear correlations between the isotopic composition ($\delta^{18}O_v$, δD_v, and d-excess$_v$), and air temperature (T), relative humidity (RH), precipitation amount (P), wind speed (WS), and dew point temperature (T_d) before, during, and after the cyclones (Table 2). Before the cyclones, both $\delta^{18}O_v$ and δD_v showed a positive correlation with air temperature (i.e., temperature effect) and dew point temperature but no correlations with other meteorological variables (Table 2). The correlation between $\delta^{18}O_v/\delta D_v$ and surface air temperature and RH became weaker during the cyclone Tauktae while much stronger (r=0.60 for temperature and r=-0.68 for RH) during Yaas. During Tauktae, we did not observe any effect of precipitation amount on the isotopic composition, while during Yaas there was a negative correlation (r=-0.56). D-excess$_v$ was positively correlated with local air temperature (negatively correlated with local RH) before, during, and after Tauktae, whilst no correlations were observed during Yaas (Table 2).

Table 2 Linear correlations between the isotopic composition of atmospheric water vapour ($\delta^{18}O_v$, δD_v, and d-excess$_v$) and air temperature (T), relative humidity (RH), precipitation amount (P), wind speed (WS), and dew point temperature (T_d) before, during, and after the cyclone events. *, **, and * indicate correlation significance levels of 0.001, 0.01, and 0.05 respectively.**

	T	RH	P	WS	T_d
Before					
$\delta^{18}O_v$	0.24***	-0.03	-0.41	-0.10	0.51***
δD_v	0.44***	0.21**	-0.37	0.08	0.63***
d-excess$_v$	0.66***	-0.64***	0.35	0.68***	0.28***
Cyclone Tauktae					
$\delta^{18}O_v$	0.15	-0.19	0.11	-0.004	0.07
δD_v	0.21*	-0.25**	0.10	0.05	0.11
d-excess$_v$	0.77***	-0.82***	-0.22	0.61***	0.51***
Cyclone Yaas					
$\delta^{18}O_v$	0.60***	-0.68***	-0.56***	0.02	0.23**
δD_v	0.63***	-0.70***	-0.56***	0.05	0.26**
d-excess$_v$	0.10	-0.006	0.19	0.32**	0.26*
After					
$\delta^{18}O_v$	0.17*	-0.19*	-	0.19*	0.09
δD_v	0.30***	-0.31***	-	0.30***	0.20*
d-excess$_v$	0.62***	-0.58***	-	0.52***	0.55***

4 ~~Discussions~~

~~To investigate the underlying factors behind the isotopic variations, we focused on the impact of moisture sources, by calculating five-day back trajectories for each day before, during, and after the cyclone events and changes of corresponding specific humidity. In addition, we explored the effects of convective activity, moisture convergence, and total rainfall along the back trajectories on water vapour isotopic depletion.~~

Formatted: No bullets or numbering

Formatted: Indent: First line: 0"

~~4.1~~3.2 Influence of Moisture source

Previous studies suggested that Kathmandu is predominantly impacted by local moisture sources with short and long-range transport of westerlies before the onset of summer monsoon, which is generally dry and characterized by sporadic rainfall with enriched $\delta^{18}O$ values in precipitation (Adhikari et al., 2020; Chhetri et al., 2014; Yu et al., 2016). We found significant proportions of moisture trajectories prior to cyclone Tauktae either originated locally or by westerlies, characterized by low specific humidity (Fig. 4~~5~~, upper left panel). These moisture trajectories were traced back to the Gangetic plain before cyclone Tauktae. The associated $\delta^{18}O_v$ and δD_v values for these moisture sources exhibited enrichment, with average values of -10.04‰ and -69.51‰ for $\delta^{18}O_v$ and δD_v, respectively. A similar slope (5.85) and intercept (-12.12) of the local meteoric vapour line before Tauktae to the surface water line calculated in the Gangetic plain (Hassenruck‐Gudipati et al., 2023) which provided corroboration for the impact of local evaporation on the isotopic composition.

As cyclone Tauktae approached the continent, the primary moisture ~~source at~~to Kathmandu was coming from the Arabian Sea, instead of local origins ~~transitioned from local origins to majority AS vapour~~ (Fig. 4~~5~~, upper right panel). The specific humidity along these trajectories exhibited higher levels over the oceans, diminishing as they traversed over land through precipitation (Fig. 4~~5~~, upper right panel). During this phase, $\delta^{18}O_v$ and δD_v were significantly lower (on average over 4.5‰ and 37‰ for $\delta^{18}O_v$ and δD_v respectively) than measurements preceding the cyclone. Such depletion can be attributed to the progressive rainout along the moisture transport path, wherein heavy isotopes are removed during successive condensation (Xu et al., 2019). Notably, the isotopic composition before the Tauktae-induced rainfall remained enriched, reflecting inflow from the surface layer (Munksgaard et al., 2015).

Furthermore, the d-excess$_v$ variation at Kathmandu during Tauktae may have been influenced by local moisture recycling processes.

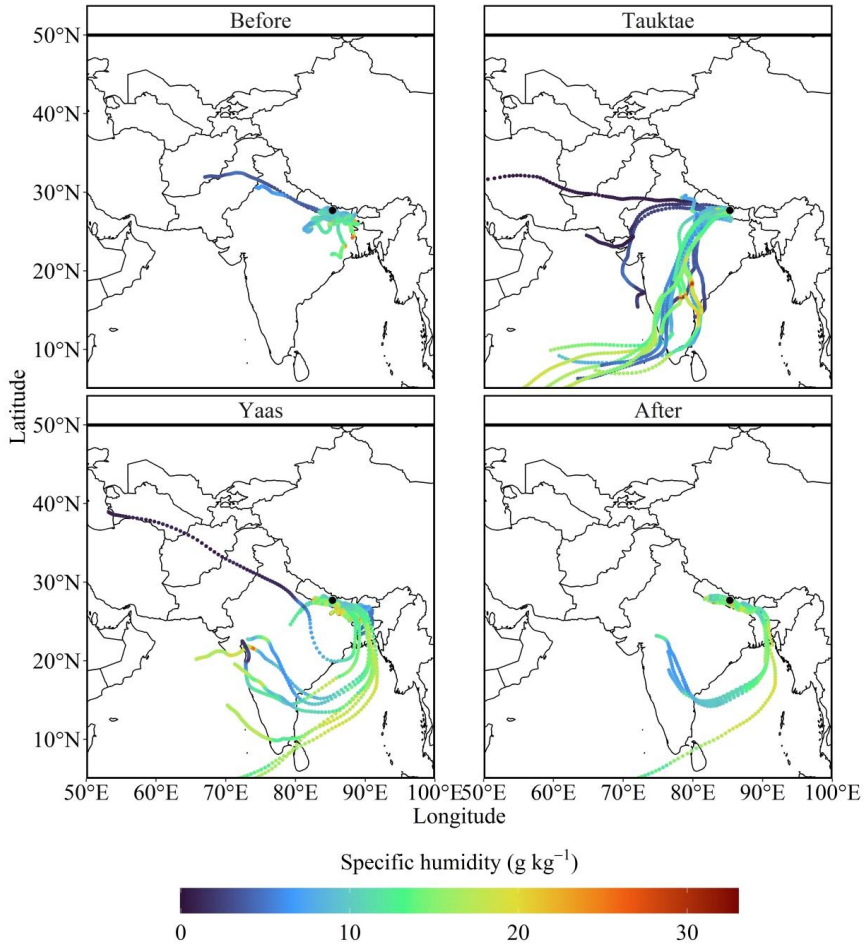

Figure 4~~5~~ Five-day backward ~~moisture~~ trajectories reaching the sampling site before, during, and after the cyclone events. Colours denote specific humidity (q in g~~/~~kg^{-1}) along the trajectories.

During cyclone Yaas, only the BoB vapour contributed to moisture at Kathmandu and specific humidity along the trajectories over the ocean was high (Fig. 4~~5~~, bottom left panel). The high specific humidity over India and surrounding regions during cyclone formation suggest that Yaas lifted a substantial amount of water vapour from the BoB yielding intense rainfall along its path. The isotopic composition during Yaas was more depleted than that of Tuaktae with averages of -17.87‰ and -129.18‰ for $\delta^{18}O_v$ and δD_v respectively. The difference could stem from varied moisture sources, rainout histories, and the respective strengths of each cyclone. Moreover, the high isotopic depletion during cyclone Yaas might be attributed to the disparity of sea surface water $\delta^{18}O$ between the AS and BoB. The surface water $\delta^{18}O$ in the BoB is relatively depleted compared to the AS (Lekshmy et al., 2014), which results from a substantial influx of freshwater from rain and runoff originating from the Ganga Brahmaputra river basin (Breitenbach et al., 2010; Singh et al., 2010).

Although, the progressive increment was seen in the time series of $\delta^{18}O_v$ and δD_v after the dissipation of Tauktae (Fig. 2~~3~~), $\delta^{18}O_v$ and δD_v in the earlier stage of Yaas were significantly lower compared to Tauktae because there was not enough time for recovery. There was a strong association between $\delta^{18}O_v$/or δD_v and local meteorological conditions during cyclone Yaas associated with high relative humidity from the remote ocean (Chen et al., 2021; Xu et al., 2019). Furthermore, the negative correlation of $\delta^{18}O_v/\delta D_v$ vs. RH and the fact that $\delta^{18}O_v/\delta D_v$ was depleted highlight the influence of humid moisture sources (Yu et al., 2008), which was also confirmed by our moisture backward trajectory analysis (Fig. 4~~5~~, bottom left panel). A similar correlation was also observed in mid-tropospheric water vapour over the western Pacific associated with intense convective activity (Noone, 2012).

In contrast to cyclone Tauktae, the lack of correlation of d-excess$_v$ with RH and local air temperature during cyclone Yaas implies that local moisture recycling processes are not significant in determining d-excess$_v$ variation and RH might not be a reliable predictor of kinetic fractionation during evaporation. Previous research conducted in the Indian Ocean (e.g., Midhun et al., 2013; Uemura et al., 2008) suggested that the high relative humidity (i.e. >80%) at the sampling sites weakens the correlation between d-excess$_v$ and RH. Our observed data also satisfied that condition during Yaas because the majority of isotopic measurements (about 75%) were associated with high relative humidity (>80%), while this fraction was only 25% during Tauktae.

Following the dissipation of the cyclones, some moisture at Kathmandu was provided by BoB vapour together with local evaporation (Fig. 4~~5~~, bottom right panel). However, the isotopic composition reverted to the original (enriched) levels ($\delta^{18}O_v$ = -11.09 ‰, δD_v= -79.38 ‰, and d-excess$_v$= 9.37 ‰). The diminished correlation between $\delta^{18}O_v/\delta D_v$ and temperature following the cyclones is attributed to the admixture of vapour originating from plant transpiration during that period (Delattre et al., 2015).

We used the vapour δD_v-q plot combined with the Rayleigh distillation and mixing curve to assess the moisture mixing (Fig. 5~~6~~). Before the development of cyclone Tauktae and during its early stages, the data points lie well above the mixing curve, indicating that the isotopic variability was mainly dominated by vapour from local evapotranspiration. In contrast, during the latter stage of cyclone Tauktae, δD_v was significantly depleted to levels well below the Rayleigh curve. During the early stage of cyclone Yaas, there are only a few data points between the mixing and Rayleigh curves with the majority well below the Rayleigh curve, particularly during the later stage. During both events, Kathmandu was dominated by deep convection

leading to a strong convergence of moisture from both the AS (Tauktae) and the BoB (Yaas). This points towards the influence of convective processes (see Section 3.3~~4.2~~) (Galewsky and Samuels-Crow, 2015). After Yaas had dissipated, δD_v gradually increased again with half of the data points clustered between the mixing and Rayleigh curves. The remaining data points were well above the mixing curve, indicating the influence of locally evaporated vapour also evidenced by the moisture back trajectories (**Error! Reference source not found.**~~Fig. 5~~4 bottom right panel).

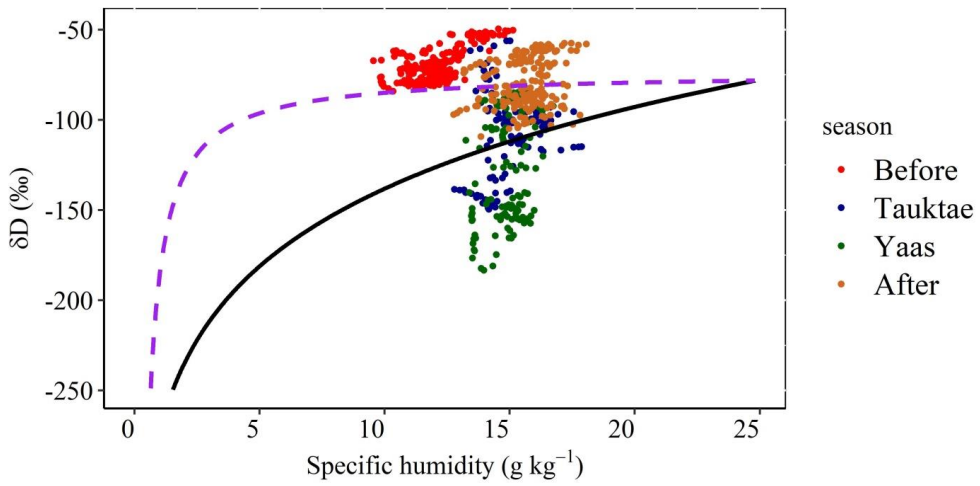

Figure 5~~6~~ Scatter plot of hourly averaged δD_v vs. specific humidity (q). The solid black curve represents the Rayleigh distillation curve calculated for the initial condition of δD_v =-78.20 ‰, BoB-averaged δD_v (Lekshmy et al., 2022), SST of 30° C, and RH of 90 %. The dashed purple~~blue~~ curve represents the mixing line, calculated based on dry continental air (q= 0.5 g~~/~~kg^{-1} and δD_v =-300 ‰ (Wang et al., 2021)) and the wet source, which corresponds to the initial conditions used to calculate the theoretical Rayleigh curve.

~~4.2~~3.3 Influence of deep convection associated with cyclones

One of the likely causes for large isotopic depletion during cyclones might be the associated convective processes. Studies have demonstrated that convective processes within tropical cyclones can cause the depleted isotopic composition of precipitation and atmospheric water vapour (Fudeyasu et al., 2008; Jackisch et al., 2022; Munksgaard et al., 2015) due to a combination of strong cyclonic circulation, intense large-scale convection, heavy precipitation, and high wind speeds (Chen et al., 2021; Xu et al., 2019). We analysed the relationship between the isotopic composition and convective processes, using OLR and vertical velocity as a proxy for convection. Due to the frequent co-occurrence of intense convection and significant mid-tropospheric convergence of moist air, the vertical velocities can also serve as a proxy for convective activity (Lekshmy et al., 2014).

Figure 6~~. S3~~ and Figure 7~~. S~~4 depict the prevalence of strong convective processes associated with both cyclones throughout their lifespan. During the initial days of cyclone formation, OLR exceeded 260 Wm^{-2} in the area of the sampling site and decreased rapidly to below 200 Wm^{-2} in the final stages of both cyclones when approaching the site. Although the amount of precipitation associated with Tauktae (9.2 mm) was much lower than Yaas (59.6 mm), $\delta^{18}O_v$ depleted by up to 12 ‰ during both cyclones. The progressive rainout was evident along the entire cyclone track (Figs. S4 and S5),, and the spatial distribution of precipitation was highly correlated with the convective process~~, as indicated by low OLR (Figs. S5 and S6),~~ suggesting rainfall occurred from the deep convective cloud rather than local evaporation. This was confirmed by precipitation variations. The site received its first rainfall on 19 May during cyclone Tauktae and on 25 May during cyclone Yaas, as shown in Figure S4~~5~~ and Figure S5~~6~~. *In situ* observations confirm that during the days leading up to cyclone Tauktae, the sampling site

455 received a total of 12.2 mm of precipitation with maximum rainfall of 9.2 mm/h recorded on 11
456 May at 13:00 h LT, equal to the total accumulated rainfall during the entire cyclone. Although
457 the pre and during-Tauktae rainfall amounts are similar, pre-cyclone $\delta^{18}O_v$ and δD_v were
458 significantly more enriched (averages: $\delta^{18}O_v$ = -10.04 ‰ and δD_v = -69.51 ‰) than during
459 Tauktae (averages: $\delta^{18}O_v$ = -14.73 ‰ and δD_v = -106.76 ‰). We compared the values of $\delta^{18}O_v$,
460 δD_v, and d-excess$_v$ during both events and also examined them in comparison with the isotopic
461 composition at the beginning of the summer monsoon (June 2021). This initial period of intense
462 and continuous rainfall at our sampling site (Fig. S6~~7~~) is regulated by the monsoon system
463 originating in the BoB. Consequently, our focus centered on the isotopic distinctions between
464 water vapour on typical rainy days and that associated with cyclone Yaas.
465

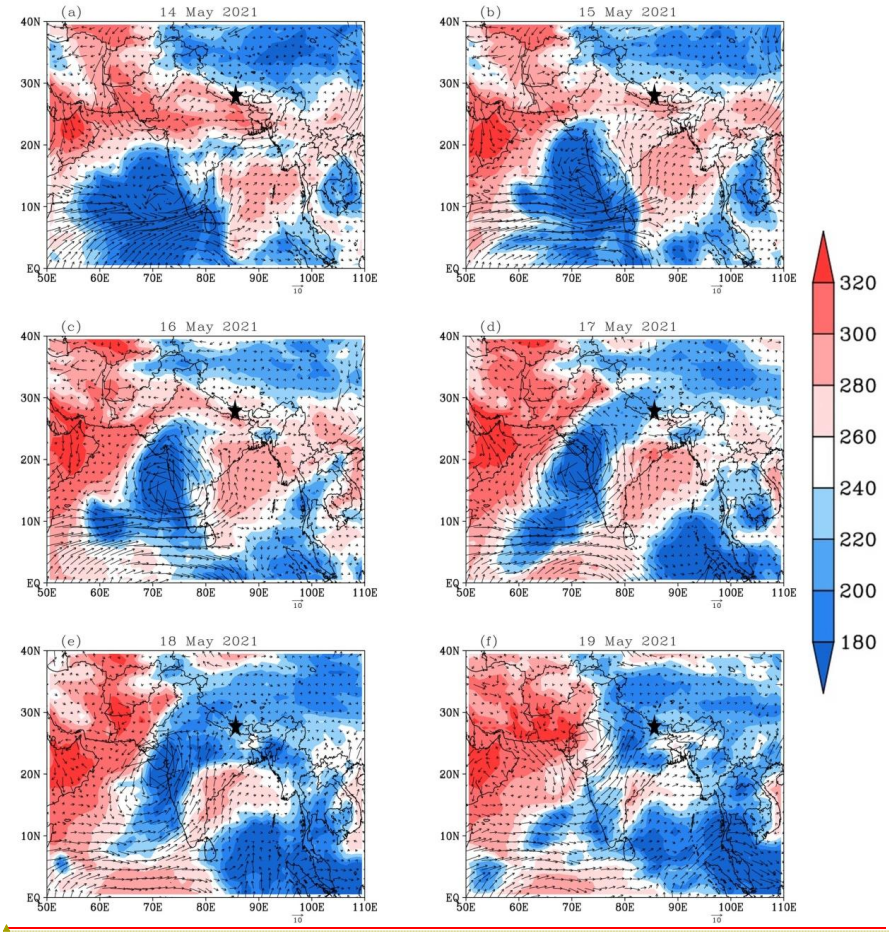

Figure 6 Regional winds (arrows) and outgoing longwave radiation (colours in Wm^{-2}) during cyclone Tauktae.

Following the initiation of the summer monsoon, both $\delta^{18}O_v$ and δD_v exhibited a progressive depletion, coinciding with a decline in air temperature, an increase in relative humidity (RH), and amplified rainfall amounts (Fig. S6~~7~~). Despite the daily accumulated rainfall and RH being significantly higher during the normal monsoon period, both $\delta^{18}O_v$ and δD_v were markedly lower during cyclone Yaas (on average by over 2.5‰ and 26‰ for $\delta^{18}O_v$ and δD_v

Formatted: Font:
Formatted: Keep with next
Formatted: Caption, Left, Indent: First line: 0", Line spacing: single

respectively) compared to typical rainy days. A progressive reduction in d-excess$_v$ was also evident as the summer monsoon unfolded; a trend typically observed in precipitation d-excess (e.g., Hussain et al., 2015; Acharya et al., 2020; Adhikari et al., 2020) and water vapour d-excess (Tian et al., 2020; Yao et al., 2018; He and Richards, 2016; Wei et al., 2016) in Asian monsoon regions, in contrast to our observations during cyclone Yaas.

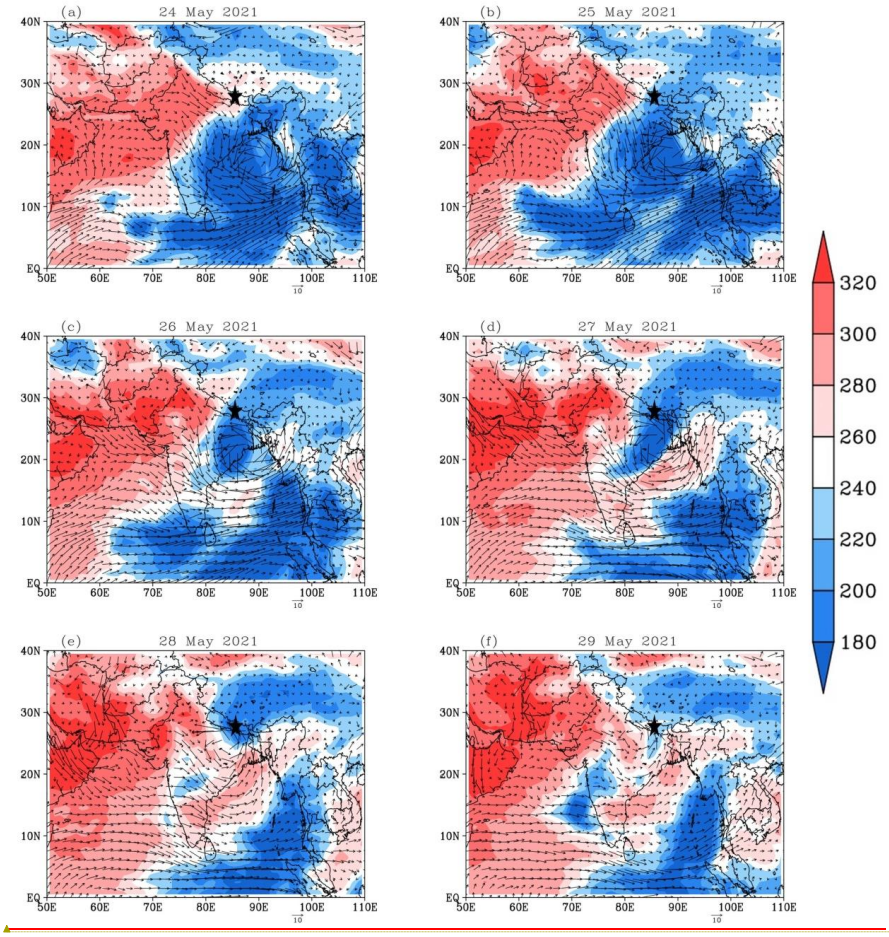

Figure 7 Same as Figure 6 but for cyclone Yaas.

Formatted: Font:

Formatted: Keep with next

Formatted: Caption, Left, Indent: First line: 0", Line spacing: single

Given that d-excess has long served as a diagnostic tool for understanding moisture source conditions (Tian et al., 2001; Liu et al., 2008), the distinct behaviour of d-excess$_v$ between cyclone Yaas and the normal monsoon phase suggests that cyclone-related information may be discerned through the isotopic composition recorded at our site. This confirms our previously stated hypothesis that rainfall associated with cyclones causes significantly lower isotope values in vapour due to intense convective systems (Gedzelman et al., 2003; Kurita, 2013), absent in local rain events and days without precipitation (Lekshmy et al., 2022).

The influence of convective processes on water vapor isotopic variations at Kathmandu is further supported by the Hovmöller diagram of OLR averaged over 80-90° E, which clearly shows that $\delta^{18}O_v$ depletion coincides with the presence of clouds (Figure ~~Fig. 7~~8b~~a~~ and c). In contrast, d-excess$_v$ showed dissimilar variations between both cyclones. Before cyclone Tauktae, the daily averaged d-excess$_v$ was above the global average of 10 ‰ (Fig. 8~~7~~a). Once Tauktae approached our sampling site, d-excess$_v$ decreased from around 12 ‰ to 10 ‰ and continued to oscillate about 10 ‰ until Tauktae had dissipated. As cyclone Yaas approached the measurement site with intense rainfall (Fig. 2~~3~~), d-excess$_v$ gradually increased while RH increased and air temperature decreased (Fig. 2~~3~~). Specifically, d-excess$_v$ on 24 May was recorded as 12.82 ‰ when surface air temperature and surface RH was about 24 $^{\circ}$C and 70 % respectively. On 27 May, we noted a 3 ‰ rise in d-excess$_v$ when the surface temperature was reduced by 4°C and the surface RH was increased by 19 %. The combination of increasing d-excess and decreasing $\delta^{18}O_v$ highlights the role of vapour recycling due to the subsidence of air masses from stratiform clouds (Kurita et al., 2011). In addition, a large increase in d-excess$_v$ was also recorded in atmospheric vapour during cyclone Ita in 2014 and was attributed to downward moisture transport above the boundary layer (Munksgaard et al., 2015). We did not find any statistically

significant correlation during cyclone Yaas between d-excess$_v$ and RH/Temperature, although RH is considered an important parameter for interpreting d-excess in atmospheric vapour and precipitation (Pfahl and Sodemann, 2014; Steen-Larsen et al., 2014). The observed co-occurrence of higher d-excess$_v$, lower temperatures, and high relative humidity (Fig. 2~~3~~) points to kinetic fractionation processes either at a larger scale or in association with downdrafts (Conroy et al., 2016). Rain re-evaporation under the condition of high saturation deficit is one of the causes of low $\delta^{18}O_v$ and high d-excess$_v$. This is due to the addition of re-evaporated vapour during precipitation events, which results in depleted cloud vapour and high d-excess$_v$ (Conroy et al., 2016; Lekshmy et al., 2014). On normal days high d-excess$_v$ values were generally accompanied by low RH (~~Fig. S7~~8) and vice versa. However, the high relative humidity of the surface air together with near saturation conditions vertically (Figure 8~~Fig. 9~~b) during cyclone Yaas, rule out any effect of re-evaporation on increased d-excess$_v$ values. Such high d-excess$_v$ values may be associated with downdrafts during convective rain events, transporting isotopically depleted vapour with higher d-excess$_v$ values from the boundary layer to the surface (Kurita, 2013; Midhun et al., 2013).

Field Code Changed

Formatted: Not Highlight

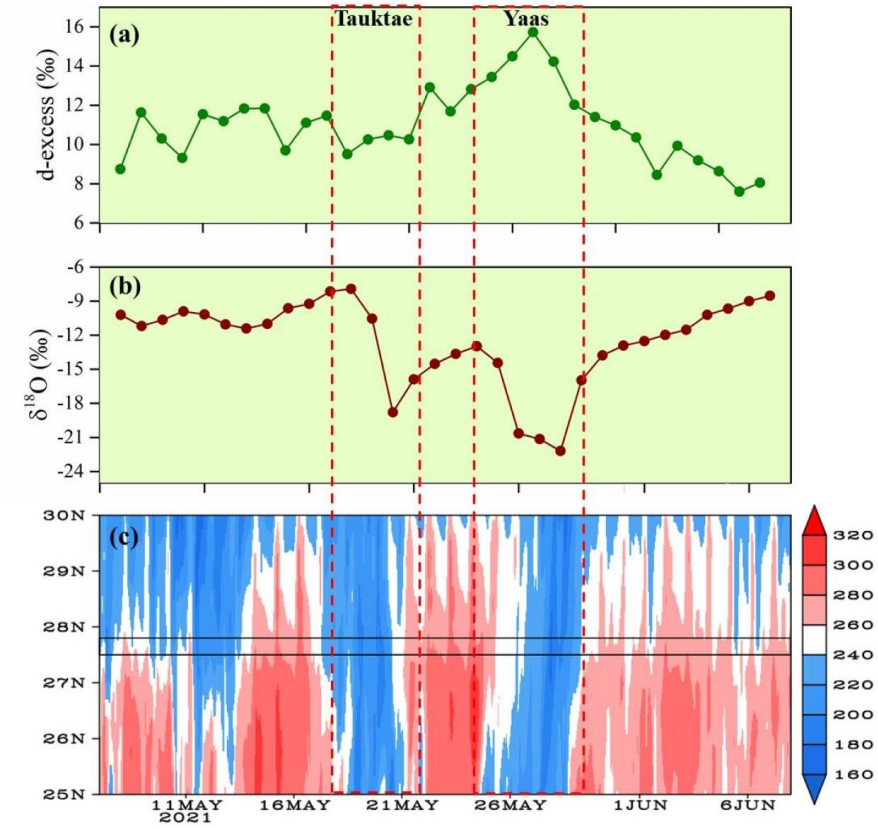

519

520 **Figure ~~7~~ 8 Time series of daily averaged d-excess$_v$ (a), $\delta^{18}O_v$ (b), and Hovmöller diagram of**

521 **OLR (W~~/~~m^{-2}~~2~~) averaged over 80° E-90° E (c) The solid parallel lines in (c) depict the**

522 **latitude range of sampling site.**

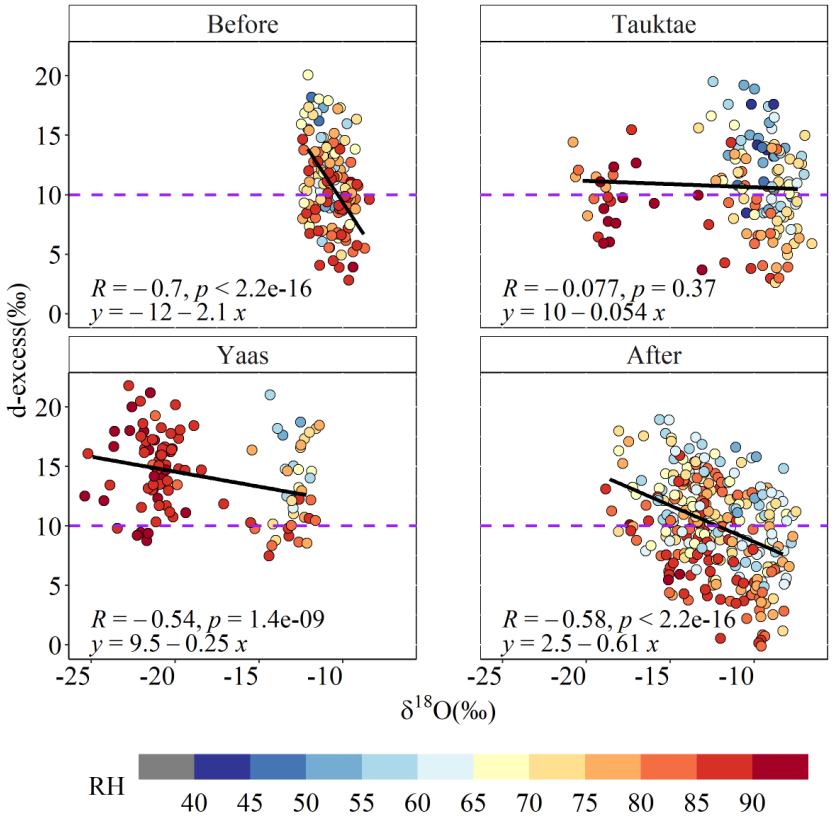

~~Figure 8 Scatter plots of d-excess$_v$ vs. $\delta^{18}O_v$ before, during, and after the cyclone events. The colour represents RH (in %) and the horizontal dashed purple lines represent the global average d-excess value (10 ‰).~~

To clarify the impact of convection on the isotopic composition, we analysed the distribution of vertical velocity, relative humidity, and air temperature averaged over a box between 25°N-28°N and 83°E-87°E with our measurement site near its center (Fig. 9). Our results show that strong shifts in $\delta^{18}O_v$, δD_v, and d-excess$_v$ during the cyclones were strongly associated with vertical air motions (Figure 8~~Fig.~~ 9c). We observed a general downward

movement of air before the rain started with Tauktae. The high depletion of $\delta^{18}O_v$ and δD_v during the final stages of Tauktae (~~Fig. 3~~2) was accompanied by strong upward air movement extending from 800 hPa to about 200 hPa (Figure 8~~Fig. 9~~c). This upward motion was even stronger during cyclone Yaas and became evident near the measurement site once Yaas made landfall on 26 May. Interestingly, variations in RH at different pressure levels strongly coincided with changes in vertical velocity while the lower troposphere remained near saturation (RH= ~100 %) during the final stages of both cyclones (Fig. 9b). While the air temperature showed the expected decline with altitude (Fig. 9a), there were no significant temporal variations during the entire period, despite the high variation in RH. The strong convective updraft added additional moisture from the warm ocean below, before passing over our measurement site (Lekshmy et al., 2014). Convective updrafts cause moisture to condense quickly and this high-efficiency condensation of heavy rain can result in more depleted $\delta^{18}O_v$ and δD_v (Lawrence and Gedzelman, 1996). In addition, we found a strong positive correlation between $\delta^{18}O_v$ and average vertical velocity (r=0.57) during Yaas at pressure levels between 300 hPa and 600 hPa (Fig. 10~~S8~~a) in the area surrounding our site. This correlation was weaker (r=0.30) during Tauktae. The distinctive relationship between $\delta^{18}O_v$ and vertical velocity implies that convective processes play a more significant role during Yaas than Tauktae. This result was further supported by the spatial distribution of correlation coefficient between $\delta^{18}O_v$ and vertical velocity (Fig. 10~~S8~~b, c). During cyclone Tauktae, a significant negative correlation was observed between $\delta^{18}O_v$ and vertical velocity around the sampling site, while positive correlation areas were identified in western Nepal, certain parts of central India, and the coastal region of the Bay of Bengal (BoB) (Fig. 10~~S8~~b). A comparison with back trajectories unveiled positive correlation only in specific sections along the moisture transport path, suggesting that convective processes

may not be the primary driver of isotopic depletion during cyclone Tauktae. Conversely, a positive correlation was evident in the coastal BoB, extending north toward the sampling site during cyclone Yaas (Fig. 10~~S8~~c). The positive correlation areas were considerably larger compared to Tauktae, and these areas closely aligned with the moisture transport path. Hence, higher depletion in $\delta^{18}O_v$ and δD_v during Yaas, relative to Tauktae, may be attributed to the stronger convection associated with BoB vapour compared to the AS vapour. The BoB is a convectively active region, and previous studies reported greater depletions in $\delta^{18}O$ and δD in precipitation, irrespective of the season (Breitenbach et al., 2010; Lekshmy et al., 2015; Midhun et al., 2018). Another reason we observed different levels of isotope depletion between both cyclones may be related to differences in their proximity to the sampling site. While Yaas came as close as 400 km to our site, Tauktae was 1100 km away when it dissipated (Fig. S8~~9~~). The proximity of Yaas may explain the stronger rainfall during that event which enhanced the isotopic fractionation in turn leading to stronger isotopic depletion (Jackisch et al., 2022). Similar results have been documented for precipitation stable isotopes (e.g., Fudeyasu et al., 2008; Jackisch et al., 2022; Munksgaard et al., 2015; Xu et al., 2019) and water vapour stable isotopes (e.g., Munksgaard et al., 2015; Rahul et al., 2016; Saranya et al., 2018). Even after both cyclones had dissipated, progressive rainfall continued at our sampling site due to the presence of residual moisture from the cyclones. Once these residual effects had diminished and rainfall intensity weakened, $\delta^{18}O_v$ and δD_v started to increase again (Fig. 2~~3~~), likely due to evaporative effects (Munksgaard et al., 2015; Xu et al., 2019; Jackisch et al., 2022).

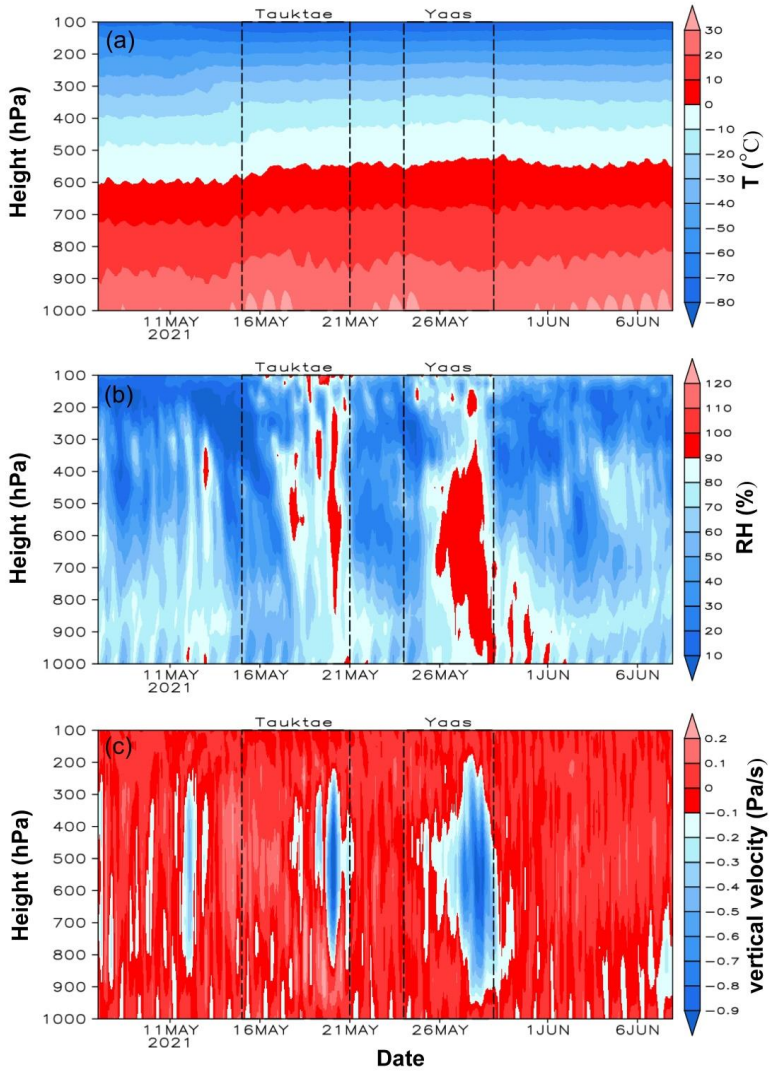

575

576 **Figure 8~~9~~ Time series of the vertical distribution of air temperature (a), RH (b), and**
577 **vertical velocity (c) averaged over 25° N-28° N and 83° E-87° E with Kathmandu**
578 **approximately at the centre. Negative (positive) vertical velocities indicate ascending**
579 **(descending) winds.**

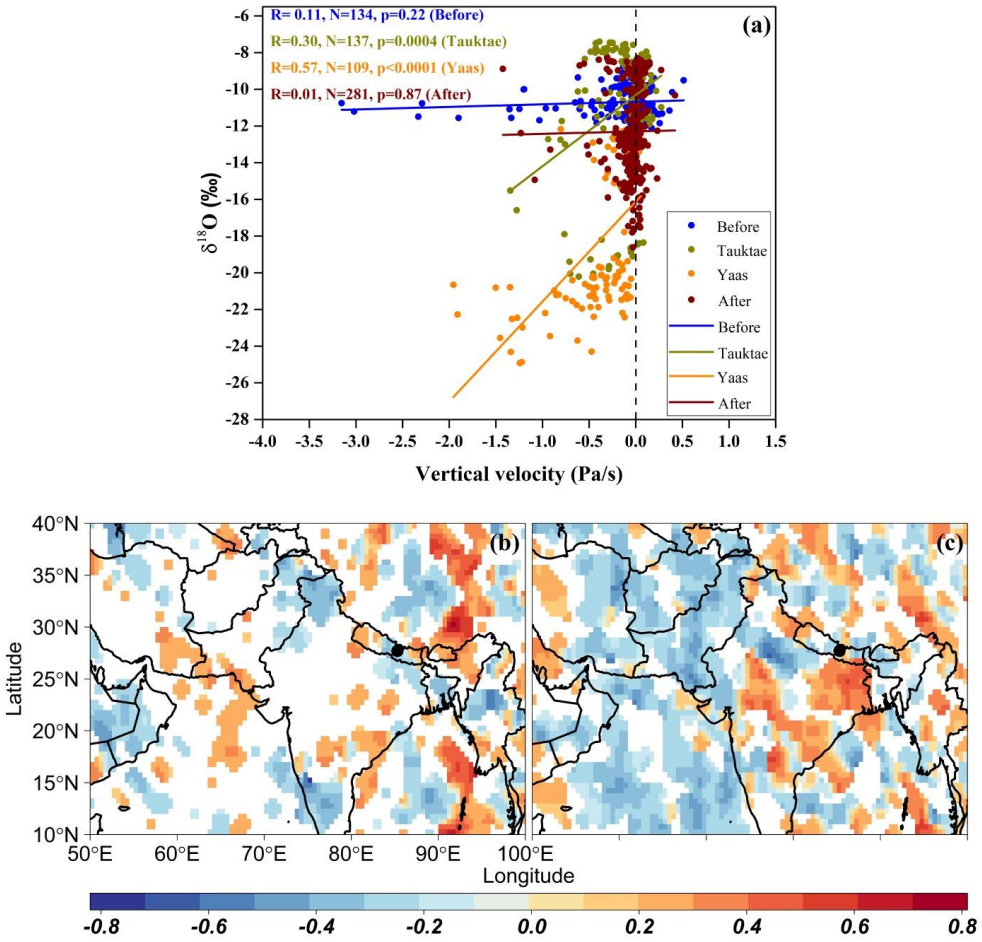

Figure 9 (a) Linear regression between $\delta^{18}O_v$ and the average vertical velocities at pressure levels between 300 hPa and 600 hPa, averaged over 25° N-28° N and 83° E-87° E which has our measurement site near its centre. (b) Spatial distribution correlation coefficient between $\delta^{18}O_v$ and vertical velocity during Tauktae. (c) Same as (b) but during Yaas. The vertical black dashed line in (a) represents the threshold separating ascending (negative values) and descending (positive values) air motions.

Formatted: Keep with next

~~4.3~~3.4 Influence of rainfall

The back trajectories reveal the impact of separate air masses during cyclones Tauktae and Yaas, specifically between the AS and BoB. We studied the meteorological conditions along the 5-day moisture back trajectories, focusing on the upstream rainout on observed isotopic depletion. During cyclone Tauktae, both $\delta^{18}O_v$ and δD_v display a strong negative correlation (r= -0.80 and r= -0.79 for $\delta^{18}O_v$ and δD_v, respectively, Fig. S9~~10~~) with total precipitation along the moisture trajectories (i.e., upstream rainout). Moreover, a negative correlation emerges between $\delta^{18}O_v/\delta D_v$ and average relative humidity (RH) along the trajectories (r= -0.69 for $\delta^{18}O_v$ and -0.68 for δD_v), suggesting increased upstream rainout corresponds to lower isotope ratios during cyclone Tauktae.

In addition, modelled back trajectories indicate that air masses during cyclone Tauktae had a longer transport time when continuous rainout could have enhanced the isotopic depletion of the residual vapour (Fig. 4, upper right panel ~~Fig. 5b~~). The upstream rainfall control could also account for the delayed return of $\delta^{18}O_v$ and δD_v to more positive values following dissipation.

Formatted: Normal

Formatted: Left, Indent: First line: 0", Line spacing: Multiple 1.15 li

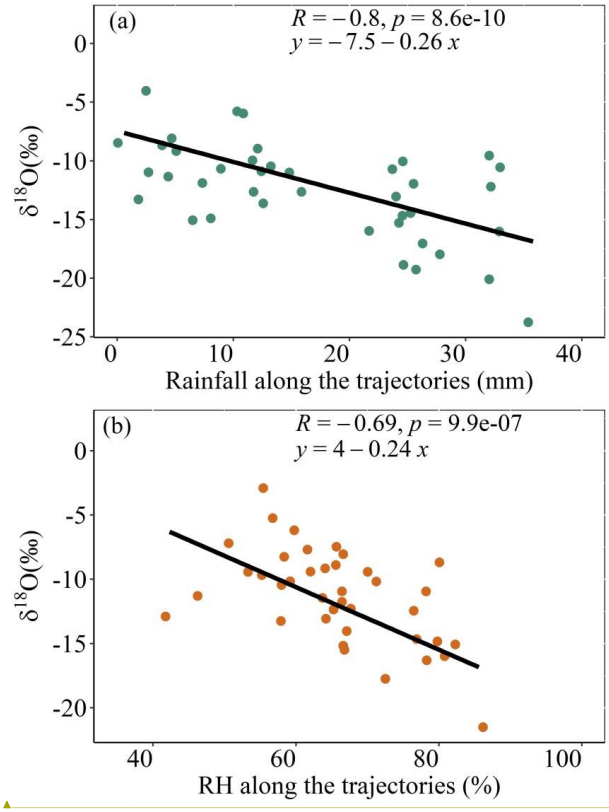

Figure 10 (a) Scatter plots of $\delta^{18}O_v$ vs upstream rainout and (b) average relative humidity (RH) along the moisture trajectories during the cyclone Tauktae.

Similar observations have been documented in other regions; for example, the Chinese Typhoons Haitang, Megi, and Soudelor (Xu et al., 2019), the Central American Hurricanes Irma and Otto (Sánchez-Murillo et al., 2019), and Central Texas Hurricane Harvey (Sun et al., 2022) all demonstrate significant negative correlations between upstream rainout and precipitation $\delta^{18}O$. This suggests that upstream rainout could serve as a widely applicable control on the spatiotemporal variability in tropical cyclones (Sun et al., 2022).

Formatted: Font: Not Bold

In contrast to cyclone Tauktae, neither the total rainfall nor the relative humidity (RH) along the trajectories appears to exert influence on isotopic variation during cyclone Yaas. Instead, a negative correlation was observed between $\delta^{18}O_v/\delta D_v$ and local rainfall amount, air temperature, and RH (Table 2). This suggests that the observed isotopic depletion during cyclone Yaas cannot be adequately explained by upstream rainout processes. We assume that sudden changes in local meteorological conditions are a consequence of synoptic processes during the cyclones. The progressive rainout during the cyclone events followed a temperature decrease (Figure 2~~Figure 2~~) which would result in the $\delta^{18}O_v/\delta D_v$ correlation with temperature (Delattre et al., 2015). The cooling of surface air during rainfall, coupled with the isotopic equilibrium of vapour with raindrops, establishes a positive correlation between $\delta^{18}O_v/\delta D_v$ and temperature (Midhun et al., 2013). These conditions were favourable during cyclone Yaas because the sampling site experienced consistent rainfall, along with a noticeable increase in relative humidity and a decrease in temperature. This might be one of the reasons for the weaker correlation of $\delta^{18}O_v/\delta D_v$ with local meteorological variables during Tauktae.

Studies have speculated that the impact of precipitation amount is not confined to a strictly local context (Galewsky et al., 2016), but is subject to modulation by convective and large-scale atmospheric properties including downdraft moisture recycling (Risi et al., 2008), large-scale organized convection and associated stratiform rain (Kurita, 2013), as well as regional circulation and shifting moisture sources (Lawrence et al., 2004). Our measurements during cyclone Yaas revealed the presence of an intense convective system over our study site, indicating that the observed effect of rainfall amount may have been governed by moisture convergence (Chakraborty et al., 2016). The subsequent rainfall originating from the convective system, occurring over a region characterized by depleted isotope values, resulted in a negative

association between precipitation amount and $\delta^{18}O_v/\delta D_v$ (Kurita, 2013). The ^{18}O-depleted water vapour reaching the sub-cloud layer, accompanied by the intense convective downdrafts, subsequently ascended back to the cloud level with the updrafts, in a feedback mechanism proposed by Lekshmy et al., (2014).

3.5 Relation with cloud-top temperature and cloud-top pressure

Formatted: Heading 2, Left, Indent: First line: 0", Line spacing: single

Given that cloud-top temperature (CTT) and cloud-top pressure (CTP) are reliable indicators of both moisture convergence and convective strength ~~in prior studies~~ (Cai et al., 2018; Cai and Tian, 2016), we investigate the linear correlation between CTT/CTP (averaged over the 27°N-28°N latitude and 85°E-86°E longitude range, with our site located at the center) and $\delta^{18}O_v$ (Fig. 11). The results demonstrate a weak positive correlation between CTT/CTP and $\delta^{18}O_v$ during cyclone Tauktae (Fig. 11a, b), and a robust positive correlation during cyclone Yaas (Fig. 11c, d). These correlations exhibit greater strength compared to the correlation observed with local rainfall. Previous research has highlighted positive correlations between $\delta^{18}O$ and CTT/CTP in the East Asian Monsoon suggesting that intense convection and moisture convergence lead to an increase in cloud-top height and a decrease in CTT, causing a reduction in $\delta^{18}O$ (Cai and Tian, 2016). The decrease in $\delta^{18}O_v$ during cyclone Yaas coupled with a decrease in CTT and CTP (i.e. increase in cloud-top height), shows the influence of intensified convective activities and moisture convergence, while the isotopic depletion during cyclone Tauktae is attributed to upstream rainout processes. Furthermore, a negative correlation is evident between d-excess$_v$ and CTT/CTP, with r = -0.52 and r = -0.60 during cyclone Yaas. Conversely, a weak positive correlation is observed during cyclone Tauktae, with r = 0.32 for both CTT and CTP. This relationship implies that lower CTT and CTP during intense convection relate to increased d-excess$_v$ values during the final stage of cyclone Yaas.

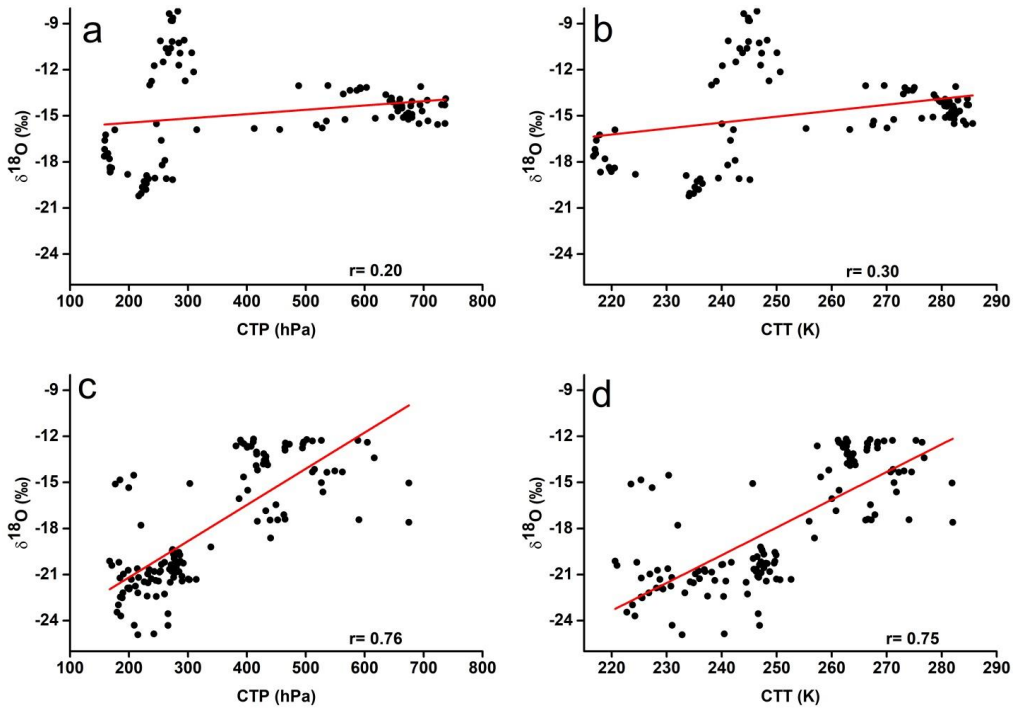

Figure 1011 Relationship between hourly $\delta^{18}O_v$ and (a) CTT during Tauktae, (b) CTP during Tauktae, (c) CTT during Yaas, and (d) CTP during Yaas.

54 Conclusion

This study presented the results of continuous measurements of the isotopic composition of atmospheric water vapour over Kathmandu between 7 May and 7 June 2021 covering two cyclone events; cyclone Tauktae formed over the Arabian Sea, and cyclone Yaas formed over the Bay of Bengal. $\delta^{18}O_v$ (δD_v) during Tauktae varied from -8.20‰ (-56.06‰) to -20.21‰ (-149.49‰) with an average of -14.73‰ (-106.76‰) and during Yaas $\delta^{18}O_v$ (δD_v) ranges from -

12.17‰ (-83.85‰) to -24.92‰ (-183.34‰) with an average of -17.87‰ (-129.18‰). Similarly, d-excess$_v$ during Tauktae varied from 7.97 ‰ to 14.24 ‰ with an average of 11.06 ‰ while during Yaas it varied from 8.71 ‰ to 18.29 ‰ with an average of 13.77 ‰. Both cyclones led to significant depletion of $\delta^{18}O_v$ and δD_v, with $\delta^{18}O_v$ decreasing by over 12 ‰. We attribute these rapid depletions to changes in moisture sources (local vs. marine) inferred from backward moisture trajectories. The lower intercepts of the local meteoric vapour line before and after the events highlight the influence of non-equilibrium processes such as evaporation on the isotopic composition. The spatial distribution of OLR, vertical velocity, and regional precipitation during both cyclonic events indicated significant moisture convergence and intense convection at and around the measurement site. This resulted in depleted $\delta^{18}O_v$ and δD_v, with cyclone Yaas exhibiting stronger moisture convergence and convection, leading to lower $\delta^{18}O_v$ values compared to cyclone Tauktae. This difference may be attributed to robust downdrafts during Yaas-related convective rain events, potentially transporting vapour with higher d-excess$_v$ and lower $\delta^{18}O_v$ values to the surface. The observed isotopic depletion during cyclone Tauktae can be explained by upstream rainout processes.~~, unlike during Yaas~~.

Overall, our results show that tropical cyclones originating in the BoB and the AS during the pre-monsoon season transport large amounts of isotopically depleted vapour and produce moderate to heavy rainfall over a sizeable region in Nepal. The isotopic composition of atmospheric water vapour and precipitation during the dry season should therefore be interpreted with caution, and the effects of cyclones should not be underestimated. In addition, our results underline the need for simultaneous measurements of the isotopic composition of both atmospheric water vapour and precipitation to better understand post-condensation exchanges between falling raindrops and boundary layer vapour over Kathmandu.

Data Availability

The data used in this study will be available in the Zenodo repository.

Competing interests

The contact author has declared that none of the authors has any competing interests.

Acknowledgements

This work was funded by 'The Second Tibetan Plateau Scientific Expedition and Research (STEP) project' (Grant No. 2019QZKK0208) and the National Natural Science Foundation of China (Grants 41922002 and 41988101-03). We thank Yulong Yang for his assistance with instrument set-up and initial running.

Author contributions

Niranjan Adhikari: Data curation, Formal analysis, Writing - Original draft preparation. **Jing Gao**: Data curation, Conceptualization, Methodology, Supervision, Writing - Review and Editing, Funding acquisition. **Aibin Zhao**: measuring assistance, Writing – Editing. **Tianli Xu**, **Manli Chen,** and **Xiaowei Niu**: measuring assistance. **Tandong Yao**: Supervision, Funding acquisition.

~~6~~5 References

Acharya, S., Yang, X., Yao, T., Shrestha, D.: Stable isotopes of precipitation in Nepal Himalaya highlight the topographic influence on moisture transport, Quat. Int., 565, 22–30, https://doi.org/10.1016/j.quaint.2020.09.052, 2020.

Adhikari, N., Gao, J., Yao, T., Yang, Y., Dai, D.: The main controls of the precipitation stable isotopes at Kathmandu, Nepal, Tellus, Ser. B Chem. Phys. Meteorol., 72, 1–17. https://doi.org/10.1080/16000889.2020.1721967, 2020

Bohlinger, P., Sorteberg, A., Sodemann, H.: Synoptic conditions and moisture sources actuating extreme precipitation in Nepal, J. Geophys. Res. Atmos., 122, 12–653, https://doi.org/10.1002/2017JD027543, 2017.

Boschi, R., Lucarini, V.: Water pathways for the Hindu-Kush-Himalaya and an analysis of three flood events, Atmosphere, 10, 489, https://doi.org/10.3390/atmos10090489, 2019.

Brand, W.A., Geilmann, H., Crosson, E.R., Rella, C.W.: Cavity ring-down spectroscopy versus high-temperature conversion isotope ratio mass spectrometry; a case study on delta (2) H and delta (18) O of pure water samples and alcohol/water mixtures, Rapid Commun. mass Spectrom, RCM 23, 1879–1884, https://doi.org/10.1002/rcm.4083, 2009.

Breitenbach, S.F.M., Adkins, J.F., Meyer, H., Marwan, N., Kumar, K.K., Haug, G.H.: Strong influence of water vapor source dynamics on stable isotopes in precipitation observed in Southern Meghalaya, NE India, Earth Planet. Sci. Lett., 292, 212–220, https://doi.org/10.1016/j.epsl.2010.01.038, 2010.

Cai, Z., Tian, L.: Atmospheric controls on seasonal and interannual variations in the

precipitation isotope in the East Asian Monsoon region, J. Clim., 29, 1339–1352. https://doi.org/10.1175/JCLI-D-15-0363.1, 2016.

Cai, Z., Tian, L., Bowen, G.J.: Spatial-seasonal patterns reveal large-scale atmospheric controls on Asian Monsoon precipitation water isotope ratios, Earth Planet. Sci. Lett., 503, 158–169. https://doi.org/10.1016/j.epsl.2018.09.028, 2018.

Chakraborty, S., Sinha, N., Chattopadhyay, R., Sengupta, S., Mohan, P.M., Datye, A.: Atmospheric controls on the precipitation isotopes over the Andaman Islands, Bay of Bengal, Sci. Rep., 6, 1–11, https://doi.org/10.1038/srep19555, 2016.

Chan, K.T.F., Chan, J.C.L., Zhang, K., Wu, Y.: Uncertainties in tropical cyclone landfall decay, npj Clim. Atmos. Sci., 5, 93, https://doi.org/10.1038/s41612-022-00320-z, 2022.

Chen, F., Huang, C., Lao, Q., Zhang, S., Chen, C., Zhou, X., Lu, X., Zhu, Q.: Typhoon Control of Precipitation Dual Isotopes in Southern China and Its Palaeoenvironmental Implications, J. Geophys. Res. Atmos., 126, 1–15, https://doi.org/10.1029/2020JD034336, 2021.

Chhetri, T.B., Yao, T., Yu, W., Ding, L., Joswiak, D., Tian, L., Devkota, L.P., Qu, D.: Stable isotopic compositions of precipitation events from Kathmandu, southern slope of the Himalayas, Chinese Sci. Bull., 59, 4838–4846, https://doi.org/10.1007/s11434-014-0547-4, 2014.

Conroy, J.L., Noone, D., Cobb, K.M., Moerman, J.W., Konecky, B.L.: Paired stable isotopologues in precipitation and vapor: A case study of the amount effect within western tropical Pacific storms, J. Geophys. Res. Atmos., 121, 3290–3303, https://doi.org/10.1002/2015JD023844, 2016.

753 Dansgaard, W.: Stable isotopes in precipitation, Tellus 16, 436–468,
754 https://doi.org/10.3402/tellusa.v16i4.8993, 1964

755 Delattre, H., Vallet-Coulomb, C., Sonzogni, C.: Deuterium excess in the atmospheric water
756 vapour of a Mediterranean coastal wetland: Regional vs. local signatures, Atmos. Chem.
757 Phys., 15, 10167–10181, https://doi.org/10.5194/acp-15-10167-2015, 2015

758 Draxler, R.R., Hess, G.D.: Description of the HYSPLIT4 modeling system, 1997.

759 Fudeyasu, H., Ichiyanagi, K., Sugimoto, A., Yoshimura, K., Ueta, A., Yamanaka, M.D., Ozawa,
760 K.: Isotope ratios of precipitation and water vapor observed in Typhoon Shanshan, J.
761 Geophys. Res. Atmos, https://doi.org/10.1029/2007JD009313, 113, 2008.

762 Galewsky, J., Samuels-Crow, K.: Summertime moisture transport to the southern South
763 American Altiplano: Constraints from in situ measurements of water vapor isotopic
764 composition, J. Clim., 28, 2635–2649, https://doi.org/10.1175/JCLI-D-14-00511.1, 2015.

765 Galewsky, J., Steen-larsen, H.C., Field, R.D., Risi, W.C., Schneider, M.: Stable isotopes in
766 athmospheric water vapor and application to the hydrologic cycle., Rev. Geophys.
767 submitted, 1–169, https://doi.org/10.1002/2015RG000512, 2016.

768 Gaona, M.F.R., Villarini, G., Zhang, W., Vecchi, G.A.: The added value of IMERG in
769 characterizing rainfall in tropical cyclones, Atmos. Res.,
770 doi:10.1016/j.atmosres.2018.03.008, 209, 95–102, 2018.

771 Gedzelman, S., Lawrence, J., Gamache, J., Black, M., Hindman, E., Black, R., Dunion, J.,
772 Willoughby, H., Zhang, X.: Probing hurricanes with stable isotopes of rain and water vapor,
773 Mon. Weather Rev, https://doi.org/10.1175/1520-0493(2003)131<1112:phwsio>2.0.co;2,

131, 1112–1127, 2003.

Han, X., Lang, Y., Wang, T., Liu, C.Q., Li, F., Wang, F., Guo, Q., Li, S., Liu, M., Wang, Y., Xu, A.: Temporal and spatial variations in stable isotopic compositions of precipitation during the typhoon Lekima (2019), China. Sci. Total Environ., 762, https://doi.org/10.1016/j.scitotenv.2020.143143, 2021

Hassenruck-Gudipati, H.J., Andermann, C., Dee, S., Brunello, C.F., Baidya, K.P., Sachse, D., Meyer, H., Hovius, N.: Moisture Sources and Pathways Determine Stable Isotope Signature of Himalayan Waters in Nepal, AGU Adv., 4, 1–19, https://doi.org/10.1029/2022av000735, 2023.

He, S., Richards, K.: Stable isotopes in monsoon precipitation and water vapour in Nagqu, Tibet, and their implications for monsoon moisture, J. Hydrol., 540, 615–622, https://doi.org/10.1016/j.jhydrol.2016.06.046, 2016.

Hersbach, H., Bell, B., Berrisford, P., Hirahara, S., Horányi, A., Muñoz-Sabater, J., Nicolas, J., Peubey, C., Radu, R., Schepers, D.: The ERA5 global reanalysis, Q. J. R. Meteorol. Soc. 146, 1999–2049, https://doi.org/10.1002/qj.3803, 2020

Hoffmann, G., Cuntz, M., Jouzel, J., Werner, M.: A systematic comparison between the IAEA/GNIP isotope network and the ECHAM 4 atmospheric general circulation model, Isot. Water Cycle Past, Present Futur. a Dev. Sci., 303–320, 2005.

Huffman, G.J., Bolvin, D., Braithwaite, D., Hsu, K., Joyce, R., Kidd, C., Nelkin, E.J., Sorooshian, S., Tan, J., Xie, P.: Algorithm Theoretical Basis Document (ATBD) of Integrated Multi-satellitE Retrievals for GPM (IMERG), version 4.6. Nasa 29, 2017.

795 Hussain, S., Xianfang, S., Hussain, I., Jianrong, L., Dong Mei, H., Li Hu, Y., Huang, W.:
796 Controlling Factors of the Stable Isotope Composition in the Precipitation of Islamabad,
797 Pakistan, Adv. Meteorol., 2015, 1-11, https://doi.org/10.1155/2015/817513, 2015.

798 Jackisch, D., Yeo, B.X., Switzer, A.D., He, S., Cantarero, D.L.M., Siringan, F.P., Goodkin, N.F.:
799 Precipitation stable isotopic signatures of tropical cyclones in Metropolitan Manila,
800 Philippines, show significant negative isotopic excursions, Nat. Hazards Earth Syst. Sci.,
801 22, 213–226, https://doi.org/10.5194/nhess-22-213-2022, 2022.

802 Joseph, S., Freeland, H.J.: Salinity variability in the Arabian Sea, Geophys. Res. Lett., 32,
803 https://doi.org/10.1029/2005GL022972, 2005.

804 Kendall, C., Caldwell, E.A.: Fundamentals of Isotope Geochemistry, Isot. Tracers Catchment
805 Hydrol., 51–86, https://doi.org/10.1016/B978-0-444-81546-0.50009-4, 1998.

806 Kleist, D.T., Parrish, D.F., Derber, J.C., Treadon, R., Wu, W.-S., Lord, S.: Introduction of the
807 GSI into the NCEP global data assimilation system, Weather Forecast., 24, 1691–1705,
808 https://doi.org/10.1175/2009waf2222201.1, 2009.

809 Knapp, K.R., Kruk, M.C., Levinson, D.H., Diamond, H.J., Neumann, C.J.: The international best
810 track archive for climate stewardship (IBTrACS) unifying tropical cyclone data, Bull. Am.
811 Meteorol. Soc., 91, 363–376, https://doi.org/10.1175/2009bams2755.1, 2010.

812 Krishnamurthy, V., Shukla, J.: Intraseasonal and seasonally persisting patterns of Indian
813 monsoon rainfall, J. Clim., 20, 3–20, https://doi.org/10.1175/jcli3981.1, 2007.

814 Kurita, N.: Water isotopic variability in response to mesoscale convective system over the
815 tropical ocean, J. Geophys. Res. Atmos., 118, 10,376-10,390,

https://doi.org/10.1002/jgrd.50754, 2013.

Kurita, N., Noone, D., Risi, C., Schmidt, G.A., Yamada, H., Yoneyama, K.: Intraseasonal isotopic variation associated with the Madden-Julian Oscillation, J. Geophys. Res. Atmos., 116, 1–20, https://doi.org/10.1029/2010JD015209, 2011.

Lawrence, J.R., Gedzelman, S.D., Dexheimer, D., Cho, H.K., Carrie, G.D., Gasparini, R., Anderson, C.R., Bowman, K.P., Biggerstaff, M.I.: Stable isotopic composition of water vapor in the tropics, J. Geophys. Res. Atmos., 109 (D6), https://doi.org/10.1029/2003jd004046, 2004.

Lawrence, J.R., Gedzelman, S.D., Gamache, J., Black, M.: Stable isotope ratios: hurricane Olivia, J. Atmos. Chem., 41, 67–82, 2002.

Lawrence, J.R., Gedzelman, S.D., Zhang, X., Arnold, R.: Stable isotope ratios of rain and vapor in 1995 hurricanes, J. Geophys. Res. Atmos., 103, 11381–11400, https://doi.org/10.1029/97jd03627, 1998.

Lawrence, R.J., Gedzelman, D.S.: Low stable isotope ratios of tropical cyclone rains, Geophys. Res. Lett., 23, 527–530, https://doi.org/10.1029/96gl00425,1996.

Lekshmy, P.R., Midhun, M., Ramesh, R.: Role of moisture transport from Western Pacific region on water vapor isotopes over the Bay of Bengal, Atmos. Res., 265, 105895, https://doi.org/10.1016/j.atmosres.2021.105895, 2022.

Lekshmy, P.R., Midhun, M., Ramesh, R.: Spatial variation of amount effect over peninsular India and Sri Lanka: Role of seasonality, Geophys. Res. Lett., 42(13), 5500–5507, https://doi.org/10.1002/2015GL064517, 2015.

837 Lekshmy, P.R., Midhun, M., Ramesh, R., Jani, R.A.: ^{18}O depletion in monsoon rain relates to
838 large scale organized convection rather than the amount of rainfall, Sci. Rep., 4, 1–5.
839 https://doi.org/10.1038/srep05661, 2014.

840 Li, L., Chakraborty, P.: Slower decay of landfalling hurricanes in a warming world, Nature 587,
841 230–234, https://doi.org/10.1038/s41586-020-2867-7, 2020.

842 Li, Z., Yu, W., Li, T., Murty, V.S.N., Tangang, F.: Bimodal character of cyclone climatology in
843 the Bay of Bengal modulated by monsoon seasonal cycle, J. Clim., 26 (3), 1033–1046,
844 https://doi.org/10.1175/jcli-d-11-00627.1, 2013.

845 Liebmann, B., Smith, C.A.: Description of a complete (interpolated) outgoing longwave
846 radiation dataset, Bull. Am. Meteorol. Soc., 77, 1275–1277, 1996.

847 Liu, Z., Tian, L., Yao, T., Yu, W.: Seasonal deuterium excess in Nagqu precipitation: Influence
848 of moisture transport and recycling in the middle of Tibetan Plateau, Environ. Geol., 55,
849 1501–1506, https://doi.org/10.1007/s00254-007-1100-4, 2008.

850 Midhun, M., Lekshmy, P.R., Ramesh, R.: Hydrogen and oxygen isotopic compositions of water
851 vapor over the Bay of Bengal during monsoon, Geophys. Res. Lett., 40, 6324–6328,
852 https://doi.org/10.1002/2013GL058181, 2013.

853 Midhun, M., Pr, L., Ramesh, R., Yoshimura, K., Kk, S.: The effect of monsoon circulation on the
854 stable isotopic composition of rainfall, J. Geophys. Res. Atmos., 123, 5205-5221,
855 https://doi.org/10.1029/2017JD027427, 2018.

856 Mohapatra, M., Srivastava, A.K., Balachandran, S., Geetha, B.: Inter-annual variation and trends
857 in Tropical Cyclones and Monsoon Depressions over the North Indian Ocean. Observed

858 Climate Variability and Change over the Indian Region, Springer Geology, 89–106,
859 https://doi.org/ 10.1007/978-981-10-2531-0_6, 2016.

860 Munksgaard, N.C., Zwart, C., Kurita, N., Bass, A., Nott, J., Bird, M.I.: Stable isotope anatomy of
861 tropical cyclone ita, North-Eastern Australia, April 2014, PLoS One 10, 1–15,
862 https://doi.org/10.1371/journal.pone.0119728, 2015.

863 Noone, D.: Pairing measurements of the water vapor isotope ratio with humidity to deduce
864 atmospheric moistening and dehydration in the tropical midtroposphere, J. Clim., 25, 4476–
865 4494, https://doi.org/10.1175/JCLI-D-11-00582.1, 2012.

866 Pandya, U., Khandelval, S., Sanghvi, H., Joshi, E., Vekaria, G.L., Jaaffrey, S.N.A., Soni, M.:
867 Cyclone 'TAUKTAE'-Observed through data & satellite images, 2021.
868 Paul, S., Chowdhury, S.: Investigation of the character and impact of tropical cyclone Yaas: a
869 study over coastal districts of West Bengal, India, Saf. Extrem. Environ., 3, 219–235,
870 https://doi.org/10.1007/s42797-021-00044-y, 2021.

871 Payne, V.H., Noone, D., Dudhia, A., Piccolo, C., Grainger, R.G.: Global satellite measurements
872 of HDO and implications for understanding the transport of water vapour into the
873 stratosphere, Q. J. R. Meteorol. Soc., 133, 1459–1471, https://doi.org/10.1002/qj, 2007.

874 Pfahl, S., Sodemann, H.: What controls deuterium excess in global precipitation? Clim. Past, 10,
875 771–781, https://doi.org/10.5194/cp-10-771-2014, 2014..

876 Rahul, P., Ghosh, P., Bhattacharya, S.K., Yoshimura, K.: Controlling factors of rainwater and
877 water vapor isotopes at Bangalore, India: Constraints from observations in 2013 Indian
878 monsoon, J. Geophys. Res., 121, 13,936-13,952, https://doi.org/10.1002/2016JD025352,

2016.

Rajeev, A., Mishra, V.: Observational evidence of increasing compound tropical cyclone-moist heat extremes in India, Earth's Futur., 10, e2022EF002992, https://doi.org/10.1029/2022ef002992, 2022.

Risi, C., Bony, S., Vimeux, F.: Influence of convective processes on the isotopic composition ($\delta^{18}O$ and δD) of precipitation and water vapor in the tropics: 2. Physical interpretation of the amount effect, J. Geophys. Res. Atmos., 113, 1–12, https://doi.org/10.1029/2008JD009943, 2008.

Sánchez-Murillo, R., Durán-Quesada, A.M., Esquivel-Hernández, G., Rojas-Cantillano, D., Birkel, C., Welsh, K., Sánchez-Llull, M., Alonso-Hernández, C.M., Tetzlaff, D., Soulsby, C., Boll, J., Kurita, N., Cobb, K.M.: Deciphering key processes controlling rainfall isotopic variability during extreme tropical cyclones, Nat. Commun., 10, 1–10, https://doi.org/10.1038/s41467-019-12062-3, 2019.

Saranya, P., Krishan, G., Rao, M.S., Kumar, S., Kumar, B.: Controls on water vapor isotopes over Roorkee, India: Impact of convective activities and depression systems, J. Hydrol., 557, 679–687, https://doi.org/10.1016/j.jhydrol.2017.12.061, 2017.

Singh, A., Jani, R.A., Ramesh, R.: Spatiotemporal variations of the δ18O–salinity relation in the northern Indian Ocean, Deep Sea Res., Part I 57 (11), 1422–1431, https://doi.org/10.1016/j.dsr.2010.08.002, 2010.

Steen-Larsen, H.C., Sveinbjörnsdottir, A.E., Peters, A.J., Masson-Delmotte, V., Guishard, M.P., Hsiao, G., Jouzel, J., Noone, D., Warren, J.K., White, J.W.C.: Climatic controls on water

vapor deuterium excess in the marine boundary layer of the North Atlantic based on 500 days of in situ, continuous measurements, Atmos. Chem. Phys., 14, 7741–7756, https://doi.org/10.5194/acp-14-7741-2014, 2014.

Sun, C., Tian, L., Shanahan, T.M., Partin, J.W., Gao, Y., Piatrunia, N., Banner, J.: Isotopic variability in tropical cyclone precipitation is controlled by Rayleigh distillation and cloud microphysics, Commun. Earth Environ., 3, https://doi.org/10.1038/s43247-022-00381-1, 2022.

Tian, L., Masson-Delmotte, V., Stievenard, M., Yao, T., Jouzel, J.: Tibetan Plateau summer monsoon northward extent revealed by measurements of water stable isotopes, J. Geophys. Res., 106, 28081–28088, https://doi.org/10.1029/2001JD900186, 2001.

Tian, L., Yu, W., Schuster, P.F., Wen, R., Cai, Z., Wang, D., Shao, L., Cui, J., Guo, X.: Control of seasonal water vapor isotope variations at Lhasa, southern Tibetan Plateau, J. Hydrol., 580, 124237, https://doi.org/10.1016/j.jhydrol.2019.124237, 2020.

Tian, L., Yao, T., Numaguti, A., Sun, W.: Stable isotope variations in monsoon precipitation on the Tibetan Plateau, J. Meteorol. Soc. Japan., 79, 959–966, https://doi.org/10.2151/jmsj.79.959, 2001.

Uemura, R., Matsui, Y., Yoshimura, K., Motoyama, H., Yoshida, N.: Evidence of deuterium excess in water vapor as an indicator of ocean surface conditions, J. Geophys. Res. Atmos., 113, https://doi.org/10.1029/2008jd010209, 2008.

Verma, K., Gupta, A., 2021. Cyclone Tauktae: Cyclones, Their Impacts and Disasters Risk Management.

921 Villarini, G., Smith, J.A., Baeck, M.L., Marchok, T., Vecchi, G.A.: Characterization of rainfall
922 distribution and flooding associated with US landfalling tropical cyclones: Analyses of
923 Hurricanes Frances, Ivan, and Jeanne (2004), J. Geophys. Res. Atmos., 116, https://doi.org
924 /10.1029/2011jd016175, 2011.

925 Wei, Z., Yoshimura, K., Okazaki, A., Ono, K., Kim, W., Yokoi, M., Lai, C.T.: Understanding
926 the variability of water isotopologues in near-surface atmospheric moisture over a humid
927 subtropical rice paddy in Tsukuba, Japan, J. Hydrol., 533, 91–102,
928 https://doi.org/10.1016/j.jhydrol.2015.11.044, 2016.

929 Worden, J., Noone, D., Bowman, K.: Importance of rain evaporation and continental convection
930 in the tropical water cycle, Nature, 445, 528–532, https://doi.org /10.1038/nature05508,
931 2007.

932 Xu, T., Sun, X., Hong, H., Wang, X., Cui, M., Lei, G., Gao, L., Liu, J., Lone, M.A., Jiang, X.:
933 Stable isotope ratios of typhoon rains in Fuzhou, Southeast China, during 2013–2017, J.
934 Hydrol., 570, 445–453, https://doi.org/10.1016/j.jhydrol.2019.01.017, 2019.

935 Yoshimura, K.: Stable Water Isotopes in Climatology, Meteorology, and Hydrology: A Review,
936 J. Meteorol. Soc. Japan, 93, 513–533, https://doi.org/10.2151/jmsj.2015-036, 2015.

937 Yu, W., Yao, T., Tian, L., Ma, Y., Ichiyanagi, K., Wang, Y., Sun, W.: Relationships
938 between $\delta^{18}O$ in precipitation and air temperature and moisture origin on a south-north
939 transect of the Tibetan Plateau, Atmos. Res., 87, 158–169,
940 https://doi.org/10.1016/j.atmosres.2007.08.004, 2008.

941 Yu W, Yao T, Tian L, Ma Y, Wen R, Devkota LP, Wang W, Qu D, Chhetri TB.: Short-term
942 variability in the dates of the Indian monsoon onset and retreat on the southern and northern
943 slopes of the central Himalayas as determined by precipitation stable isotopes, Clim. Dyn.,
944 47, 159-72, https://doi:10.1007/s00382-015-2829-1, 2016.

945

946

947